



저작자표시-비영리-변경금지 2.0 대한민국

이용자는 아래의 조건을 따르는 경우에 한하여 자유롭게

- 이 저작물을 복제, 배포, 전송, 전시, 공연 및 방송할 수 있습니다.

다음과 같은 조건을 따라야 합니다:



저작자표시. 귀하는 원저작자를 표시하여야 합니다.



비영리. 귀하는 이 저작물을 영리 목적으로 이용할 수 없습니다.



변경금지. 귀하는 이 저작물을 개작, 변형 또는 가공할 수 없습니다.

- 귀하는, 이 저작물의 재이용이나 배포의 경우, 이 저작물에 적용된 이용허락조건을 명확하게 나타내어야 합니다.
- 저작권자로부터 별도의 허가를 받으면 이러한 조건들은 적용되지 않습니다.

저작권법에 따른 이용자의 권리는 위의 내용에 의하여 영향을 받지 않습니다.

이것은 [이용허락규약\(Legal Code\)](#)을 이해하기 쉽게 요약한 것입니다.

[Disclaimer](#)

공학박사 학위논문

성장인자 장기방출형 의료용 티타늄 임플란트

**Biomedical Titanium Implants
Eluting Growth Factors
for Long Period Time**

2013년 2월

서울대학교 대학원

재료공학부

정현도

Abstract

Biomedical Titanium Implants Eluting Growth Factors for Long Period Time

Hyun-Do Jung

Department of Materials Science and Engineering
Seoul National University

Titanium (Ti) is one of the most frequently used biomaterial in the orthopedic and dental field due to their outstanding mechanical properties, chemical stability, and good biocompatibility. Despite these excellent properties and extensive usage in the medical field, titanium has limited bone integrative properties prolonged when exposed in physiological environment. As attempts to overcome this problem, researchers in the past decade have utilized biomolecules such as growth factors to coat the implant to enhance the bone and implant integration. One of the most commonly researched biomolecule is bone Morphogenetic Protein-2 (BMP-2). BMP-2 is an osteogenic protein that plays an important role in physiological functions such as embryonic development, generation of the central nervous system, and tissue repair. However, BMP-2 coated on Ti surfaces often results in rapid diffusion, denaturation and degradation. Therefore a novel BMP-2 carrier is

needed to release BMP-2 for an extended period.

In the first study, Ti scaffolds were fabricated through a novel freeze casting method for use as Ti-based BMP-2 carriers. Dynamic freeze casting was used to produce porous Ti scaffolds with a uniform porous structure and good ductility. Ti/camphene slurries with various initial Ti contents (15, 20, and 25 vol%) were frozen at 44 °C in rotation, in which camphene crystal growth occurred extensively and uniform Ti walls were constructed. All fabricated samples showed spherical pores surrounded by dense Ti walls that were uniformly formed. The porosity decreased from 71 to 52 % with an increase in Ti content from 15 to 25 vol%, whereas the pore size decreased from 362 to 95 μm . The compressive strength and stiffness increased considerably from 57 to 183 MPa and from 1.3 to 5.0 GPa, respectively. These results indicate that dynamic freeze casting is quite useful for producing porous Ti scaffolds with a uniform pore structure which has a potential for use as bone scaffold materials.

In the second study, Ti scaffolds fabricated by dynamic freeze casting were studied for their abilities to load and deliver growth factor such as BMP-2. Porous Ti scaffold was soaked in a solution containing BMP-2 in a vacuum state and was densified to control the release rate of BMP-2. By SEM observation, porosity and pore size of the densified Ti decreased with an increase in pressure. The tensile strengths of the densified scaffolds range from 44 to 164 MPa, which are similar to the mechanical properties of the human cortical bone. GFP was used to analyze the growth factor loading capability of the densified Ti samples. Through CLSM imaging, the densified titanium samples showed prolonged release of the loaded GFP which were

slowly released from the internal pores up to 16 weeks. The release of BMP-2 from the BMP-2-embedded densified Ti was relatively steady in which considerable amounts of BMP-2 were released even after 20 weeks. The in vitro cellular responses of the MC3T3-E1 pre-osteoblasts were examined using a cell attachment, a cell proliferation assay and an alkaline phosphatase (ALP) assay, and these results demonstrated that the BMP-2 embedded densified Ti also enhanced cell adhesion, proliferation and differentiation levels. Additional cell tests were performed to verify the functionality of BMP-2 after 8 weeks of release. To examine the potential of BMP-2-embedded densified Ti as a growth factor carrier, in vivo animal test was conducted using a rabbit calvarial defect model. The micro-CT images of BMP-2-embedded densified Ti ring implant that was implanted for 6 weeks showed better integration with the calvaria on the surface compared to the as-received Ti implant. Moreover, better cell ingrowth was observed on the densified sample compared to that of the control sample. The new bone volume of the densified samples was approximately 1.5 times greater than that of the as-received control sample. These results suggest that that BMP-2 embedded densified Ti could be used as a potential candidate for the growth factor delivery systems in the dental and orthopedic field.

Keywords: Titanium, Porous Metal, Freeze Casting, Biocompatibility, Sustained Release, BMP-2

Student Number: 2008-20686

Contents

Abstract	i
List of Tables	vii
List of Figures	
Chapter 1. Introduction (Theoretical Review)	1
1.1 Metallic biomaterial as bone graft substitute	2
1.1.1 Bone graft substitute.....	2
1.2 Growth factor delivery system	5
1.2.1 BMP as a growth factor.....	5
1.2.2 Growth factor delivery	7
1.3 Porous titanium	8
1.3.1 Methods for fabrication of porous titanium	8
1.3.2 A novel technique to produce porous titanium: freeze casting	12
Chapter 2. Dynamic Freeze Casting for the Production of Porous Titanium	26
2.1 Introduction	27

2.2 Experimental Procedure	28
2.2.1 Material Preparation	28
2.2.2 Characterization	29
2.2.3 Mechanical properties	30
2.3 Results and discussion	30
2.3.1 Characterization	30
2.3.2 Mechanical properties	33
2.4 Conclusions	35

Chapter 3. Sustained Release of BMP-2 from Densified Titanium Scaffold	50
3.1 Introduction	51
3.2 Experimental Procedure	52
3.2.1 Material Preparation	53
3.2.2 Characterization	53
3.2.3 Mechanical properties	54
3.2.4 <i>In vitro</i> tests.....	54
3.2.5 <i>In vivo</i> tests.....	57
3.3. Results and Discussion	59

3.3.1 Characterization	59
3.3.2 Mechanical properties	60
3.3.3 <i>In vitro</i> tests.....	61
3.3.4 <i>In vivo</i> tests.....	67
3.4. Conclusions	70
Chapter 4. Conclusions	92
References	95
Bibliography	110
Abstract (Korean)	115

List of Tables

Table 1. Growth factors commonly used in tissue engineering.

Table 2. Overview of the merits and drawbacks of porous Ti and Ti alloys made by various methods.

Table 3. Summary of the freezing and boiling points of solvents used for unidirectional freezing.

Table 4. Oxygen, hydrogen, and carbon concentration of the porous Ti scaffold produced with an initial Ti content of 15 vol%.

Table 5. Porosity and pore size of the porous Ti scaffolds produced with various initial Ti contents (15, 20, and 25 vol%).

Table 6. Porosity and pore size of the porous Ti scaffolds used in the experiment.

Table 7. Porosity and pore size of the densified Ti scaffolds with various pressure conditions.

List of Figures

Figure 1. Degranulating platelets resulting from fracture or osteotomy release growth factors and recruit mesenchymal cells.

Figure 2. BMPs (specific growth factors) promote differentiation of mesenchymal cells toward bone formation.

Figure 3. The production of porous Ti alloy by positive sponge replication.

Figure 4. SEM micrograph of reticulated Ti–6Al–4V foam produced by sintering of powders deposited onto a temporary polyurethane scaffold [22].

Figure 5. SEM micrograph of the porous titanium foam fabricated using the space holder method [23].

Figure 6. Process of making porous Ti alloy using 3-D fiber deposition.

Figure 7. Schematic illustrations showing (A) the freezing behavior of the alumina/camphene slurry and (B) the bicontinuous structure formed by the camphene dendrite growth [47].

Figure 8. Schematic diagram illustrating the creation of large interconnected pores using dynamic freeze casting.

Figure 9. Optical images illustrating the green body of the dynamic freeze casting process.

Figure 10. Typical optical image of the porous Ti scaffolds produced with various initial Ti contents (15, 20 and 25 vol%).

Figure 11. Micro-CT images of the porous Ti scaffolds produced with (A) conventional freeze casting and (B) dynamic freeze casting.

Figure 12. SEM images of the porous Ti scaffolds produced with various initial Ti contents of (A) 15, (B) 20, and (C) 25 vol%.

Figure 13. SEM images showing the Ti walls of the porous Ti scaffolds produced (A) with and (B) without the CIP process (Initial Ti content = 15 vol%).

Figure 14. Typical X-ray diffraction patterns of the sintered sample with an initial Ti content of 15 vol%.

Figure 15. Typical EDS spectrum of the porous Ti scaffold produced with an initial Ti content of 15 vol%.

Figure 16. Pore size distributions for the porous Ti scaffolds produced with various initial Ti contents of (A) 15, (B) 20, and (C) 25 vol%.

Figure 17. Typical compressive stress versus strain responses of the porous Ti scaffolds produced with various initial Ti contents (15, 20, and 25 vol%).

Figure 18. Compressive strength and stiffness of the porous Ti scaffolds as a function of the initial Ti content.

Figure 19. Rabbit calvarial implants and their surgical placements. (A) Ring type porous Ti implant, densified titanium after pressing and as-received Ti (B) Two implants were placed side by side into the calvaria of each rabbit randomly. (C) Representative rabbit calvaria images retrieved 6 weeks after implantation

Figure 20. Optical image of the Ti scaffolds with increasing uniaxial pressings.

Figure 21. SEM images of the Ti scaffolds with increasing uniaxial pressings; (A) w/o pressing, (B) 500 MPa, (C) 1000 MPa and (D) 2000 MPa.

Figure 22. Micro-CT images of the Ti scaffolds with increasing uniaxial pressings; (A) w/o pressing, (B) 500 MPa, (C) 1000 MPa and (D) 2000 MPa.

Figure 23. Tensile strength of the dense Ti scaffolds as a function of the initial porosity.

Figure 24. Typical CLSM images of GFP loaded Ti scaffolds at 0, 14, 28, 56 and 112 days post-loading. (A) GFP-adsorbed as-received Ti, (B) GFP-loaded porous Ti and (C) GFP-embedded densified Ti.

Figure 25. Typical optical image of the porous densified Ti scaffolds (A) P71, (B) P60, (C) P52 and (D) P43) and (E) D71, (F) D60, (G) D52 and (H) D43 produced with various initial porosities.

Figure 26. Cumulative amounts of BMP-2 released from the as-received, porous and densified Ti as a function of time (n = 5).

Figure 27. Schematic of sustained growth factor release from densified Ti scaffold.

Figure 28. Typical optical images of the 52% porous Ti scaffolds with varying densifications: (A) as is, (B) densified to 42%, (C) 24% and (D) 7%.

Figure 29. Cumulative amounts of BMP-2 released from densified Ti scaffolds as a function of time (n = 5).

Figure 30. CLSM images of cellular attachment of the (A) as-received Ti, (B) BMP-2-adsorbed as-received Ti and (C) BMP-2-embedded densified Ti after culturing for 3 h.

Figure 31. Cell proliferation level of MC3T3-E1 cells of as-received Ti, BMP-2-adsorbed as-received Ti and BMP-2-embedded densified Ti after culturing for 3 and 5 days, *p < 0.05.

Figure 32. ALP activity level of MC3T3-E1 cells of as-received Ti, BMP-2-adsorbed as-received Ti and BMP-2-embedded densified Ti after culturing for 10 days, *p < 0.05.

Figure 33. Cell proliferation level of MC3T3-E1 cells of well without BMP-2 (negative control), with BMP-2 (positive control), and with released BMP-2 collected periodically after culturing for 3 and 5 days.

Figure 34. ALP activity of MC3T3-E1 cells of well without BMP-2 (negative control), with BMP-2 (positive control), and with released BMP-2 collected periodically after culturing for 10 days, *p < 0.05.

Figure 35. Micro-CT cross-section of a representative rabbit calvaria after 6 weeks of healing (A) as-received Ti (control), (B) BMP-2-adsorbed as-received Ti and (C) BMP-2-embedded densified Ti.

Figure 36. Micro-CT 3-D reconstructions of the rabbit calvaria and implants retrieved at 6 weeks after implantation. (A) as-received Ti (control), (B) BMP-2-adsorbed as-received Ti and (C) BMP-2-embedded densified Ti.

Figure 37. (A) The new bone volume was separately quantitated for the interior, calvarial side of the ring implant and the total space of ring implant as shown in the diagram. (B) The average volume of new bone in the interior, calvarial side of the implant and total space of the ring implants for the three different types at 6 weeks determined by micro-CT, *p < 0.05.

Chapter 1.
Introduction (Theoretical Review)

1.1 Metallic biomaterial as bone graft substitute

1.1.1 Bone graft substitute

When bones are fractured or damaged, the most widely practiced clinical therapies for the bone replacement include autologous and allogenic bone grafts. Autologous bone graft utilizes bone harvested from the patients' bodies. Autologous bone graft is widely used for achieving a bony bridge between two transverse processes such as spinal fusions. On the other hand, allogenic bone grafts are grafts using tissues from the same species. In order to fully understand the bone autogenous transplantation, one needs to understand the following terms: (1) osteogenesis: the process in which bone settles and grows as a result of osteoblastic activity, (2) osteoinduction: the process in which osteogenesis is stimulated. Bone morphogenic proteins (BMPs), belong to the transforming growth factor- β (TGF- β) family, are present in the bone grafts and they activate the differentiation process of the mesenchymal cells to osteoblasts [1, 2]. The cells that are capable of differentiating into osteoblasts can be found in the recipient bone, periosteum, or differentiated from vascular pericytes. Platelet-derived growth factors, on the other hand, are released from degranulating platelets in fracture hematomas and stimulate macrophages to release additional growth factors, (3) osteoconduction: is the process in which bone grows on the material surface. The implanted matrix provides surface for bone cell deposition and provides temporary support while the bone regeneration occurs. Often times, bone marrow aspirate is used in conjunction with other bone graft substitutes to provide osteoinduction (bone marrow aspirate) and

osteoconduction (such as ceramic scaffolds) as shown in Figures 1 and 2.

Understanding the biological properties of bone and transplant repair is equally important. Bone is composed of cortical and cancellous bone. The cortical bone is the outer layer of bone that is relatively harder and dense and the cancellous (spongy or trabecular) bone comprises the interior of the bone that is more porous. The rate of which bone deposition occurs differs for cancellous and cortical autografts. Cancellous bone experience faster deposition due to the living cells and greater porosity. The surface area of the cancellous bone is much larger than that of the cortical bone; therefore, the rate of regeneration of bones is much faster than the cortical bone. However, the cortical graft provides mechanical support. Therefore, when larger grafts are used (i.e. for bone tumors), cortical grafts can provide the structural support while the bone regeneration occurs. Generally, resorption occurs around the periphery of the graft, and this may affect the strength of the graft until remodeling occurs [3].

The general consensus is that bone autograft mentioned above make it the preferred choice when biological materials are needed to aid the regeneration procedure[4, 5]. However, the usage of these materials comes with several risks such as donor site morbidity, chronic post-operative pain, hypersensitivity and infection that are inherent with the secondary operation that is required to remove the material [6-10]. In addition, there is only a limited availability of autografts which limits the usage. On the other hand, allogeneic grafts are abundant and do not require an additional surgery on the patient. A disadvantage of allogenic grafts is that they have to undergo numerous treatments such as lyophilization, irradiation or freeze-drying to

avoid immunogenic reaction through removing the immunogenic proteins [11]. These processing techniques negatively affect the osteoinductive and osteoconductive potentials of allografts which consequently decreases the biological performances [12, 13].

These disadvantages of allografts and autografts encouraged the study and development of synthetic materials for orthopedic surgeries. Bone-mimetic materials such as calcium phosphates based ceramics and cements have composition and architecture that is similar to that of the bone. Ceramics have many appealing qualities for use as biomaterials. However, the usage of ceramics in the medical field is limited to non-load-bearing applications due to their brittle fracture properties. Polymeric biomaterials are another possible alternative for use as implant materials. Its ductile nature is an attractive quality as a biomaterial but it lacks structural rigidity that is required for bone replacement [14, 15].

The disadvantages of ceramics and polymeric materials have made metals the best alternative for long-term load-bearing applications. Metals have many advantages with their excellent mechanical strength and resilience when compared to alternative biomaterials, such as polymers and ceramics. The most widely used biomaterial is titanium (Ti) and its alloys. Ti has been a popular material in orthopedic and dental devices because of their excellent mechanical properties and biocompatibility [16, 17].

1.1.2 Background on metallic biomaterials

Metallic biomaterials have the longest history among various materials used for implant devices. Historical records show that the usage of

metals for medical applications was simultaneously developed around the world with the acquisition of Western science and expansion of civilizations[16]. In the 1950's, stainless steel was first successfully used as an implant material [18]. Then, vitallium, a cobalt-based alloy was put into practical use. The “newest” metallic biomaterials include Ti, stainless steel, and cobal-based alloys. These are the most commonly used materials in modern medical practices.

Titanium-based metals have been extensively used in orthopedic and dental implants for decades [19]. Among the biomaterials available, titanium-based materials are most widely used for implantation due to the combination of its outstanding characteristics such as high strength, low density (high specific strength), high immunity to corrosion, complete inertness to the body environment, enhanced biocompatibility, low modulus and high capacity to join with bone and other tissues [20]. Despite these excellent properties and extensive usage in the medical field, titanium has limited bone integrative properties in physiological environment. To overcome this problem, studies in the past decade have utilized affinity technology and coated Ti implants with biomolecules such as growth factors to enhance the bone and implant integration.

1.2 Growth factor delivery system

1.2.1 BMP as a growth factor

Growth factors are polypeptides that are secreted by cells to transmit signals that activate specific developmental programs that regulate

cell migration, differentiation, and proliferation. Growth factors such as fibroblast growth factors (FGFs), transforming growth factors (TGFs), bone morphogenetic proteins (BMPs) and vascular endothelial growth factors (VEGFs) are commonly known as being associated with the stimulation of wound healing, bone regeneration and angiogenesis as shown in Table 1.

Growth factors involved in bone formation and regeneration have been identified, and members of the TGFs superfamily clearly play an important role. TGFs generally influences the early stage of bone development, as well as bone repair and remodeling after trauma, through regulating mesenchymal precursor cells proliferation and differentiation [21]. Among others, bone morphogenetic proteins (BMPs), which are members of the TGFs superfamily, are of great interest in the orthopedic research.

Initially BMPs were thought to be involved in direct ectopic bone formation. However, modern day research as shown that BMPs are now known to be involved in so many other developmental processes as well that several investigators have suggested to change the name to Body Morphogenetic Proteins [22, 23]. The BMPs are subdivided into groups based on their sequence similarity and known functions. BMPs are typically divided into at least four subgroups: BMP 2/4, BMP 5/6/7/8a/8b, BMP 9/10, and BMP 12/13/14 [24, 25]. The individual functions of the BMPs were studied by gene manipulation technique. BMPs 2, 4, 8b, and 10 are embryonic lethal in homozygous nulls with the embryonic stage of lethality which indicates their involvement in preceding processes [26, 27]. Complicating interpretation of phenotypes are compensatory functional overlaps so dual or multiple deletions were necessary in some cases [28, 29].

Embryonic lethality also precluded establishing function in postnatal development and adult tissue homeostasis, requiring conditional knockouts [30]. BMP-2 through BMP-8 are osteogenic proteins that play essential roles in embryonic development, generation of the central nervous system, and tissue repair [31, 32].

1.2.2 Growth factor delivery

Many have focused on developing appropriate carriers for localized BMP delivery. Collagen-based carriers are a popular choice for bone induction since collagen is a major non-mineral component of the bone. Recombinant forms of collagen have been used as carriers for BMP delivery for spine fusion in humans [33]. Synthetic polymeric systems made of poly (lactide-co-glycolide) (PLG) in forms of porous scaffolds and capsules have also been used for rhBMP-2 delivery to improve the control of the rate of BMP release [34, 35]. Injectable systems of polyethylene glycol hydrogels and PLG microspheres delivering BMP-2 have also been studied and showed that they promoted osteoblast differentiation and mineralization *in vitro*, and ectopic bone formation *in vivo* [36, 37].

As described above, polymers have been widely used as BMP carriers even though metals are more appropriate for the load-bearing applications. When metal are used as a BMP carrier, the release of the protein are very rapid [38]. Therefore, to compensate for the quick release, coating layers with micro pores or polymeric materials have been used to sustain growth factor release [39, 40]. Some researchers have discovered that growth factor can be loaded from the porous materials [38, 41]. The usage of

porous materials as biomaterials has many advantages. Among them, the most important one is that the surface area of the material is much larger than that of the dense body and it also provides a biomimetic structure making it.

1.3 Porous titanium

1.3.1 Methods for fabrication of porous titanium

Thus far, a variety of manufacturing methods have been investigated to produce porous Ti scaffolds. It is difficult to process Ti when it is at liquid state due to its high melting point and high contamination susceptibility. Therefore, powder metallurgy is more frequently used to fabricate porous Ti. A number of processes have been applied to produce porous Ti and Ti alloy implants. Generally these different methods can be classified into three methods: replication, space holder method and rapid prototyping.

1.3.1.1 Replication technique

Replication is a technique that uses a three-step procedure to produce highly porous materials, as depicted in Figure 3. Li et al. utilized this method to produce porous titanium structures [42]. Polyurethane foams were dipped in a slurry comprising Ti powder (70% wt), H₂O (20% wt) and ammonia solution. The role of ammonia solution is to improve the rheological properties of the slurry. The soaked sample was subsequently dried and the process was repeated until all the struts of the foam were coated with Ti-6Al-4V powder. The final step is to remove the polyurethane

scaffold and the binder through a thermal treatment and sintering of the structure, which results in a reticulated open-cell foam with hollow titanium struts, as illustrated in Figure 4.

1.3.1.2 Space holder technique

The space holder method is a fabrication process that can produce porous metal samples of high porosity as well. The mixture of metal powders with space holder material is uniaxially or isostatically compacted to form a green body. The resulting pellet is then heat treated at a low temperature to remove the space holder, which also initiates early stage sintering of the metal particles that are in contact and forms necks. Continued sintering at higher temperatures allows these necks to grow. This leads to a densification of the structure and consequently improves the structural integrity. One of the requirements for this procedure is that the powder size of the metal powder should be smaller than the average powder size of the space holder. In addition, the pressure for compacting the metal powder and the space holder mixture must be high enough to provide the structure with sufficient mechanical strength to retain its geometry throughout the foaming process. This method produces a foam with a close to homogenous pore structure and high levels of porosity (60–80%) [43]. The mechanical properties of the metal foam can be tailored by varying the size, shape and quantity of the space holder. An example of the porosity that can be achieved using this process is shown in Figure 5. The inevitable difficulty of this method is the removal of large quantities of the space holder materials from the compacted mixture. Bram et al. used carbamide

(urea) powders, which could be removed at temperatures below 200 °C, with minimal contamination of the titanium powders.

1.3.1.3. Rapid prototyping technique

Recently, a novel three-dimensional printing (3DP) process has been used to create porous implants with controlled size, shape and distribution of the porosity [44, 45]. 3-DP is a rapid prototyping (RP) technology that creates complex three-dimensional parts directly utilizing a computer model of the part with no need for other tooling. The sequence of operations is depicted in Figure 6. A slicing algorithm is used to subdivide the computer model into many layers and prints the material accordingly layer by layer approach which allows for fabrication of complex 3-D shapes. Parts are created inside a cavity that contains a powder bed supported by the moving piston. Each new layer is fabricated through lowering of the piston by a layer thickness and filling the resulting gap with a thin distribution of powder. The method is similar to ink-jet printing technology, in which a binder material selectively joins powder particles at sites where they have to be welded. The layering process is repeated until the whole part is completed. As the final step, heat treatment is used to consolidate the part and the unbound powder is removed.

1.3.1.4. Others

(1) Particle sintering

Porous coatings and porous bulk materials can be produced by sintering uniformly sized beads under isostatic pressing or loose packing [46,

47]. The volume fraction of porosity is associated with the degree of particle interconnectivity and the particle size, and it can be controlled by altering the process variables such as compacted powder density, sintering temperature and time, and alloying additions. This method results in: (i) a low porosity (generally less than 50%), (ii) difficulty in controlling pore size, which is dependent on shape and size of the particles and (iii) incomplete interconnectivity of pores.

(2) Fiber and wire mesh

Galante et al. [48] first reported on the animal testing of sintered fiber metal composites consisting of short Ti fibers. The procedure is similar to particle sintering with the difference that fibers or wire mesh are used instead of particles. The major disadvantage of the metal fiber sintered porous coatings compared to the coatings made by powder metallurgy techniques is that fibers must be compacted prior to sintering. It is therefore difficult to coat complex shapes that do not allow compaction forces to be applied directly on the fibers. Another disadvantage of this method is the potential of inadequate coating-to-substrate contact due to insufficient fiber compaction. In addition, the porosity of the metal fiber coatings is limited to 30–50% by volume, which consequently limits bone ingrowth.

(3) Plasma spraying

Hahn and Palich first reported a plasma-sprayed Ti coating for fabricating porous-coated implants [49]. Ti hydride powders are fed into a plasma flame, whereby the decomposed Ti is deposited onto the target substrate. In general, Ti powder is sprayed onto the surface of an implant under reduced pressure condition in an inert gas chamber at a high

temperature. This deposition results in a coating layer with an irregularly shaped porous surface. Plasma spraying was also used to make bulk Ti implants and implants with a gradual change in porosity from the interface to the coated surface [50-52]. The drawbacks of the plasma spraying are the poor interconnectivity of the pores and the relatively small pore sizes.

(4) Foaming by H₂O₂

Another method to produce porous Ti body is through a foaming method. In this method, Ti powder is mixed with an organic solvent to make Ti slurry, to which H₂O₂ is subsequently added as a foaming agent which creates pores within the slurry. The pore size and porosity can be adjusted by controlling the amount of H₂O₂ added to the slurry [53]. A limitation of the method is the inability to control the porosity and interconnectivity.

(5) Argon expansion process

In this processing technique, compressed argon gas is entrapped in a Ti body during heat-compaction of Ti powders; the resulting argon bubbles are then expanded by exposure to high temperature, in which the densified Ti matrix creeps [54, 55].

A brief description and comparison of the methods to produce porous Ti and its alloys are summarized in Table 2. Porous Ti materials produced using different techniques have shown successful clinical results [56, 57]. However, from the overview above, it is obvious that there is room for further improvement of the existing production methods.

1.3.2 A novel technique to produce porous titanium: freeze casting

A relatively new method to produce porous titanium is freeze casting. Freeze casting is an easy and cost effective technique for preparing porous materials. Crystals of water or organic solvent can be generated by freeze casting, then they can be removed by thawing or direct sublimation at low temperature and in vacuum state to create pores [58, 59]. A structure with pore channels or fibers can be prepared using this technique. The pore morphology solely depends on the crystal morphology. Currently reported crystal formations types include lamellar, rods, cells and dendrites.

For the freeze casting and freeze-drying, the solvent has to satisfy two conditions: it must be frozen at moderately low temperature and the sublimation of the solvent crystal under reasonable temperature and pressure has to be achievable. Up to now, water, camphene, 1,4-dioxane, tert-butyl alcohol, benzene, dichloroethane and liquid CO₂ were used for freeze casting [59-63]. Freezing temperature and boiling temperature of the aforementioned solvents are summarized in Table 3.

1.3.2.1 Camphene based freeze casting

In this study, we used the camphene freeze casting method to achieve ultra-high porosity and completely interconnected pore channels, because of its advantages over the aqueous freeze casting technique. First, the solid loading in the ceramic slurry was minimized to achieve ultra high porosity. For the case of aqueous freeze casting, the frozen ice has to be removed via vacuum drying, which often damages the green sample either during or after the removal process. However, the frozen camphene can be removed via sublimation without the assistance of suction, which is

advantageous for lower solid loading. Second, camphene normally produces large circular pore channels which prevent the decline in permeability that is often caused by the formation of narrow interconnections, while water creates flat ellipsoidal pore channels due to the strong anisotropic growth kinetics of hexagonal ice crystals [64-66]. Third, the freezing process can be carried out at near room temperature, due to the moderate solidification temperature of camphene (T_m : 44°–48°C), thus allowing a more flexible working conditions.

Schematic illustrations of the camphene-based freeze casting technique are shown in Figure 7 [67]. Using the warm ball-milling process at 60 °C, it is possible to homogeneously disperse the ceramic powders in the molten camphene with the aid of a dispersant. Immediately after freeze casting at 20 °C, the molten camphene starts to freeze and grows dendritically, and simultaneously, the ceramic powders containing the dispersant are expelled by the growing camphene and become concentrated between the camphene dendrites as shown in Figure 7 (A). This freezing behavior results in the formation of a bicontinuous structure, in which each separated phase (camphene or concentrated ceramic powder network) is interconnected in 3-D space as illustrated in Figure 7 (B). It should be emphasized that the ceramic walls have high green densities of >50 vol%, regardless of the initial solid loading, which makes it possible to produce dense ceramic walls after sintering, without disturbing the 3-D pore structure [66].

Recently, freeze casting of an aqueous slurry has emerged as a promising method for producing metal foams, especially Ti foams with

aligned, elongated pores, which can be created after removing the ice dendrites that have grown unidirectionally during directional solidification [68, 69]. Special care should be taken to minimize the oxygen contamination originating from the starting Ti particles and water since it can make the foams brittle. In efforts to lower the oxygen content, our group proposed camphene as an alternative freezing vehicle, which would not react with TiH_2 and Ti particles [70-72].

Both freeze casting methods often suffer from the considerable sedimentation of relatively large Ti particles during solidification, resulting in an inhomogeneous porous structure. More specifically, when fine particles (e.g. ceramic particles) are used as starting materials, they can be sufficiently stabilized using a dispersant, allowing homogenous porous structure to be formed [65, 73, 74]. However, in the case of relatively coarse particles (e.g. commercial Ti particles), they tend to settle in a freezing vehicle before the slurry can be fully solidified, causing undesirable density and porosity gradients [75]. Thus, it is still a challenge to explore new ways of achieving a homogenous distribution of relatively large Ti particles within the slurry during freeze casting.

In this dissertation, an innovative way to produce homogeneous porous structure is introduced and the mechanism of dynamic freeze casting is investigated. The research was extended to combine a novel growth factor delivery system with porous Ti produced by dynamic freeze casting to develop a therapeutic biomaterial. The biocompatibility and the effectiveness of the loaded growth factors were evaluated by *in vitro* and *in vivo* tests.

Table 1. Growth factors commonly used in tissue engineering

Growth factor	Abbreviation	Molecular weight (kDa)	Known functions
Epidermal growth factor	EGF	6.2	Proliferation of epithelial, mesenchymal, and fibroblast cells
Platelet-derived growth factor	PDGF-AA	28.5	Proliferation and chemoattractant agent for smooth muscle cells; extracellular matrix synthesis and deposition
	PDGF-AB	25.5	
	PDGF-BB	24.3	
Transforming growth factor- α	TGF- α	5.5	Migration and proliferation of keratinocytes; extracellular matrix synthesis and deposition
Transforming growth factor- β	TGF- β	25.0	Proliferation and differentiation of bone forming cells; chemoattractant for fibroblasts
Bone morphogenetic protein	BMP-2	26.0	Differentiation and migration of bone forming cells
	BMP-7	31.5	
Basic fibroblast growth factor	bFGF/FGF-2	17.2	Proliferation of fibroblasts and initiation of angiogenesis
Vascular endothelial growth factor	VEGF	38.2	Migration, proliferation, and survival of endothelial cells

Table 2. Overview of merits and drawbacks of the porous Ti and Ti alloys made by various methods

Method	Advantages	Drawbacks	Reference
Replication	<ul style="list-style-type: none"> • Porosity up to 80% • Relatively simple to produce 	<ul style="list-style-type: none"> • Brittle foam 	[22]
Space holder	<ul style="list-style-type: none"> • Relatively simple method • Porosity up to 80% • Controllable pore size and porosity 	<ul style="list-style-type: none"> • Difficult to control pore interconnectivity • Many closed pores 	[23]
Rapid prototyping	<ul style="list-style-type: none"> • Easy to control pore size 	<ul style="list-style-type: none"> • Non-cost effective methods • Non-spherical pore shape 	[24, 25]
Particle sintering	<ul style="list-style-type: none"> • Relatively simple to produce • Interconnected pores • Narrow pore size distribution 	<ul style="list-style-type: none"> • Low porosity (<45%) • Pore size as function of particle size 	[26, 27]
Fiber and wire mesh	<ul style="list-style-type: none"> • Interconnected pores 	<ul style="list-style-type: none"> • Relatively difficult to produce • Low porosity 	[28]
Plasma spraying	<ul style="list-style-type: none"> • Commercially most successful for surface-coating 	<ul style="list-style-type: none"> • Lack of interconnected pores • Small pore size • Variable porosity 	[29-32]
Foaming by H ₂ O ₂	<ul style="list-style-type: none"> • Relatively simple method 	<ul style="list-style-type: none"> • Low porosity • Non-controllable pore size • Poor pore interconnectivity 	[33]
Argon expansion process	-	<ul style="list-style-type: none"> • Low porosity • Poor pore interconnectivity 	[34-37]

Table 3. Summary of the freezing and boiling points of solvents used for unidirectional freezing

Solvent	Freezing point (°r)	Boiling point (°o)
Water	0.0	100.0
1,4-Dioxane	11.8	101.1
Tert-butyl alcohol	25.7	82.4
Benzene	5.5	80.1
Diethyl ether	-35.0	83.5
Camphene	44.0-48.0	159.0

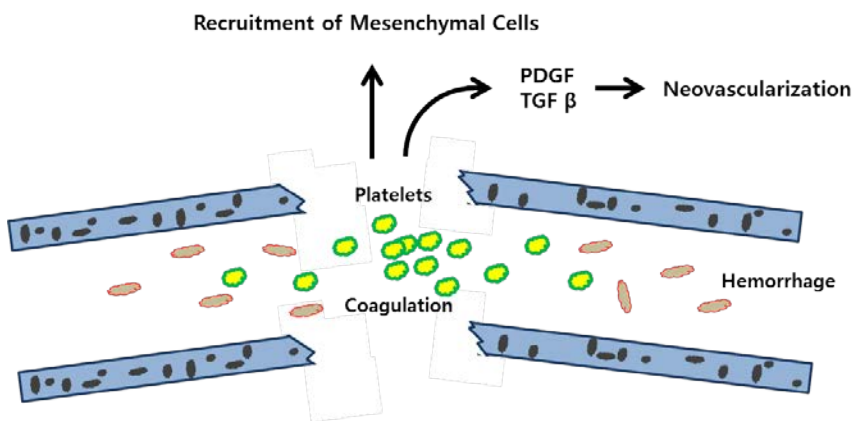


Figure 1. Degranulating platelets resulting from fracture or osteotomy release growth factors and recruit mesenchymal cells. PDGF indicates platelet-derived growth factors; TGF- β , transforming growth factor- β .

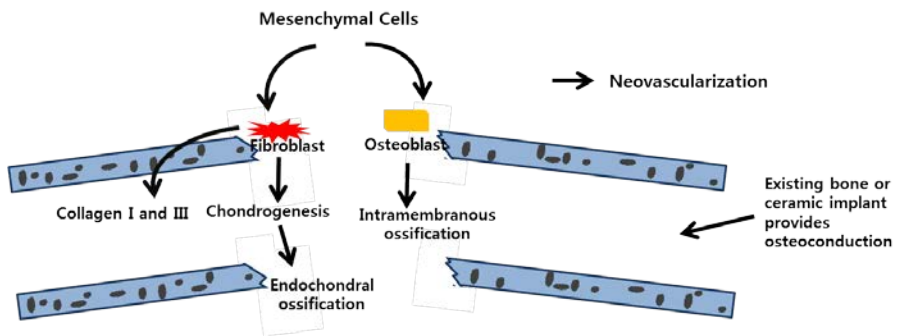


Figure 2. BMPs (specific growth factors) promote differentiation of mesenchymal cells toward bone formation. BMP indicates bone morphogenic proteins.

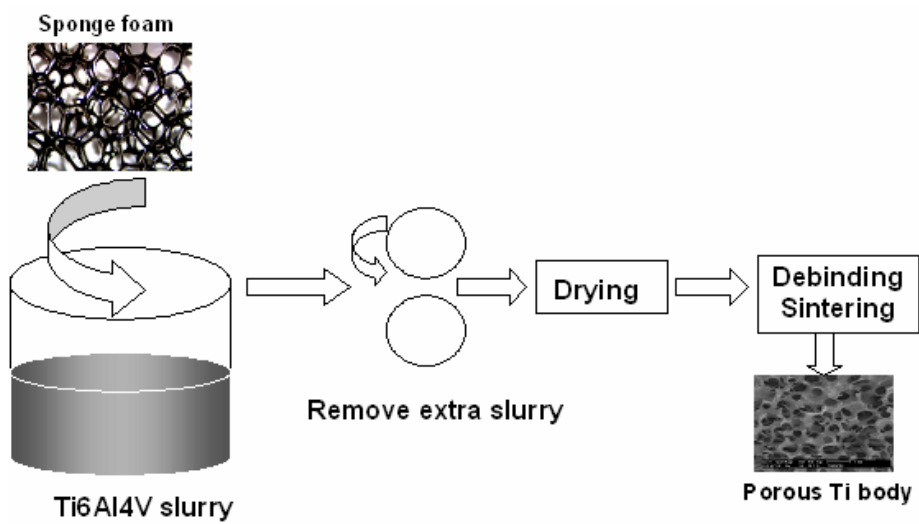


Figure 3. The process of porous Ti alloy production by positive sponge replication.

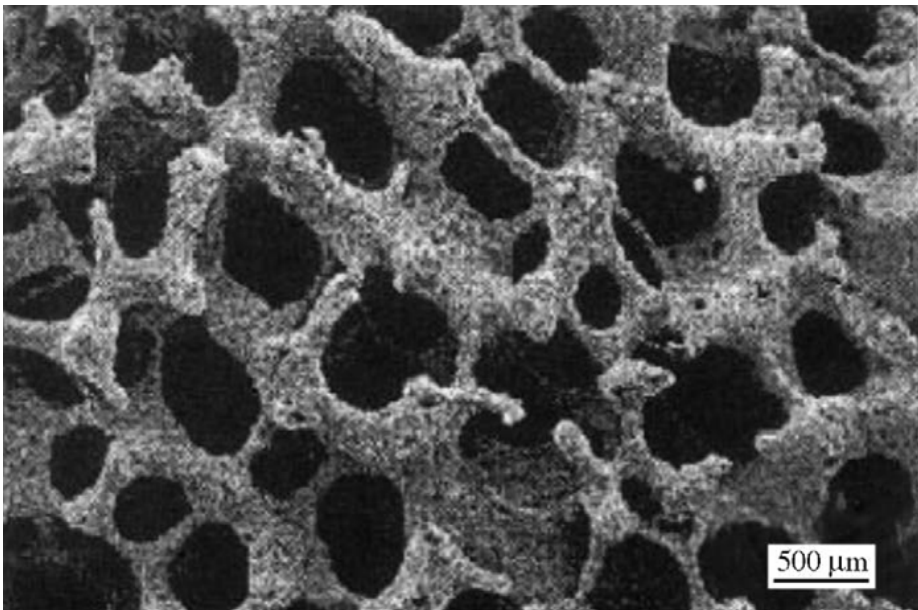


Figure 4. SEM micrograph of reticulated Ti-6Al-4V foam produced by sintering of powders deposited onto a temporary polyurethane scaffold [22].

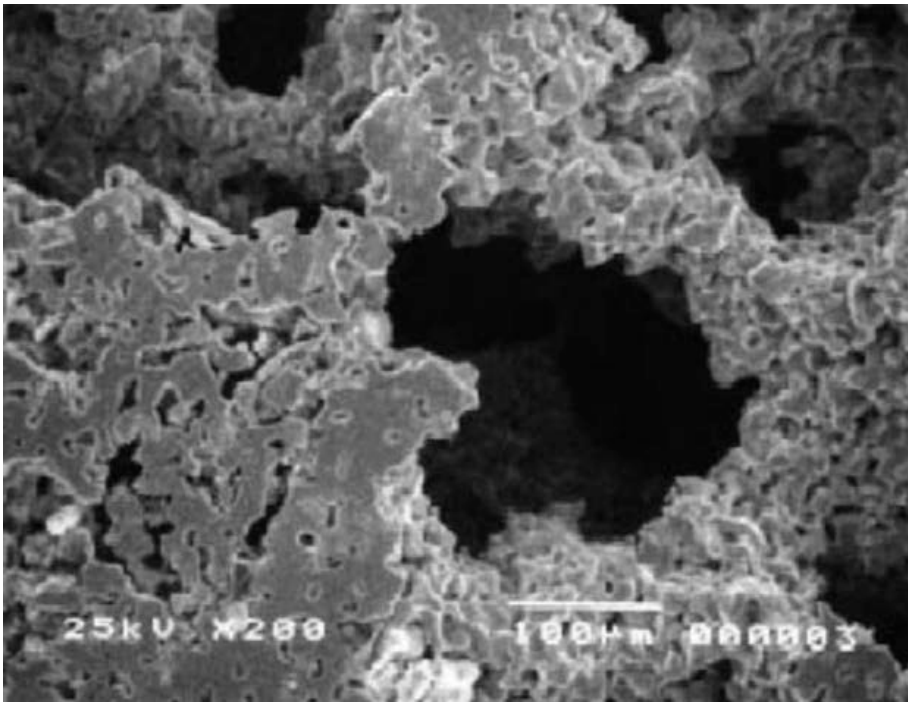


Figure 5. SEM micrograph of the porous titanium foam fabricated using the space holder method [23].

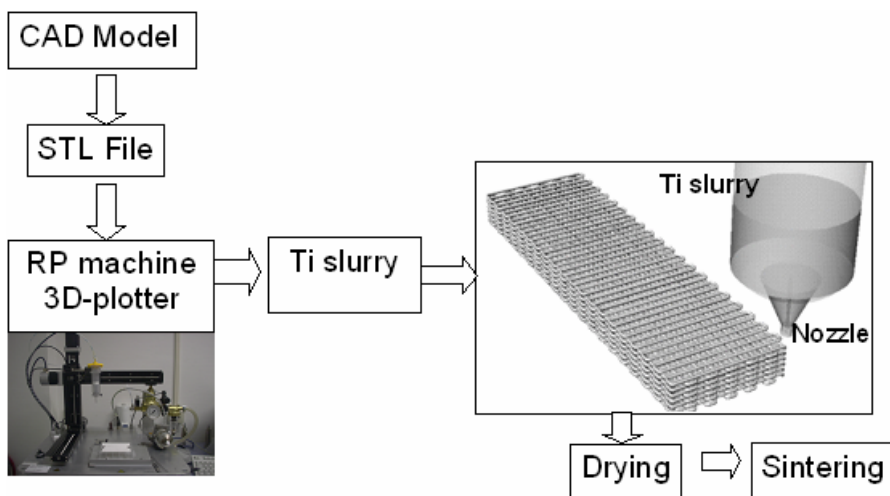


Figure 6. Process of making porous Ti alloy using 3-D fiber deposition.

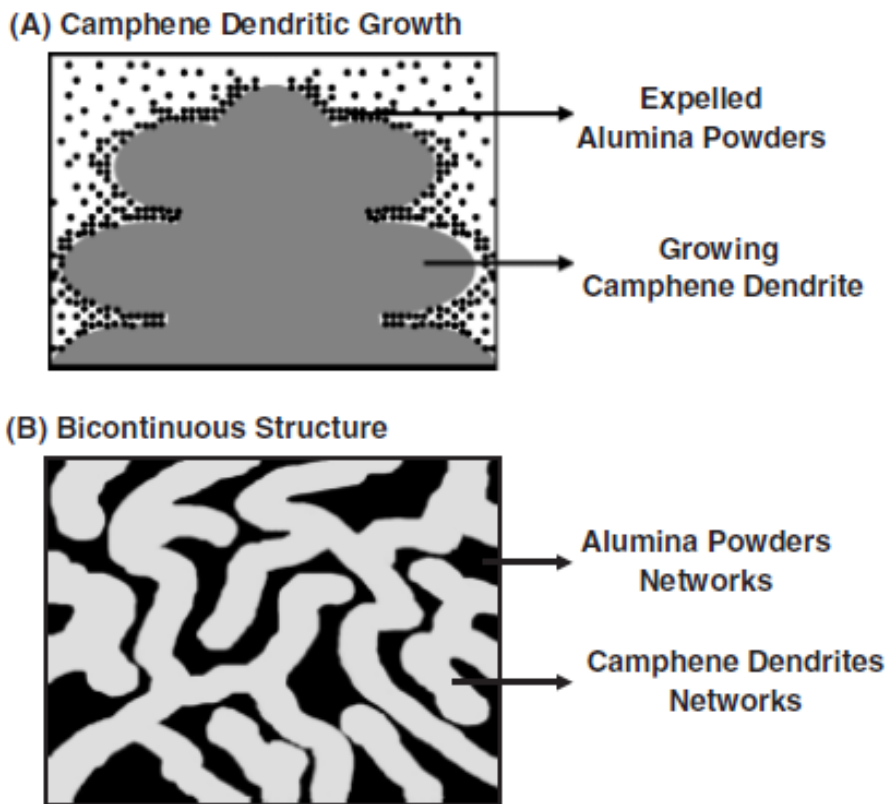


Figure 7. Schematic illustrations showing (A) the freezing behavior of the alumina/camphene slurry and (B) the bicontinuous structure formed by the camphene dendrite growth [47].

Chapter 2.
Dynamic Freeze Casting for the
Production of Porous Titanium

2.1 Introduction

Titanium (Ti) and its alloys are one of the most widely used materials in the medical field as orthopedic and dental implants due to their excellent mechanical properties, chemical stability, and good biocompatibility [17, 76]. In addition, these materials with a porous structure have attracted increasing interest, because the 3-dimensional pore network can provide a favorable environment for bone ingrowth and the porous materials possess bone-like mechanical properties [77, 78]. Thus far, considerable efforts have been made to develop new manufacturing techniques for producing porous Ti scaffolds, such as replication of polymeric sponge, sintering of metal particles, rapid prototyping (RP) method and space holder method [79-82].

Recently, freeze casting of an aqueous slurry has emerged as a promising method for producing Ti foams with aligned, elongated pores, which can be created after removing the ice dendrites grown unidirectionally during directional solidification [68, 69]. Special care should be taken to avoid the embrittlement of porous Ti foams, which is caused by oxygen contamination originating from the starting Ti particles and water. Therefore to lower the oxygen content, our group proposed camphene as an alternative freezing vehicle, which would not react with TiH_2 and Ti particles [70-72].

Both freeze casting methods often suffer from the considerable sedimentation of relatively large Ti particles during solidification, resulting in an inhomogeneous porous structure. More specifically, when fine particles (e.g. ceramic particles) are used as starting materials, they can be sufficiently stabilized by a dispersant, allowing a homogenous porous

structure. However, in the case of relatively coarse particles (e.g. commercial Ti particles), they tend to settle in a freezing vehicle before the slurry can be fully solidified, causing undesirable density and porosity gradients [75]. Thus, it is still a challenge to explore new ways of achieving a homogenous distribution of relatively large Ti particles in a slurry during freeze casting.

This study reports how porous Ti scaffolds can be produced with a uniform porous structure by freezing Ti/camphene slurry in rotation at 44 °C for 12 h, which is denoted as “dynamic freeze casting”. The porous structure, chemical composition and crystalline structure of the fabricated porous Ti scaffolds were characterized. Compressive strength tests were also carried out to evaluate the mechanical properties of the porous Ti scaffolds.

2.2 Experimental Procedure

2.2.1 Material Preparation

Commercially available titanium (Ti) powder (-325 mesh, Alfa Aesar, Ward Hill, MA, USA) and camphene (C₁₀H₁₆, Sigma Aldrich, St. Louis, MO, USA) were used as the starting materials. Titanium (Ti)/camphene slurries with a variety of initial Ti contents (15, 20, and 25 vol%) were prepared by ball-milling at 55 °C for 30 min with the assistance of 1 wt% of oligomeric polyester (Hypermer KD-4; UniQema, Everburg, Belgium) as a dispersant. Subsequently, the prepared slurries were transferred to cylindrical aluminum (Al) molds, 60 mm in diameter and 60 mm in height, and continuously rotated at a speed of 30 rpm, which was determined empirically, for preventing particles sedimentation. Relatively

low and high rotation speed would cause the severe segregation of the Ti particles because of the gravity and centrifugal force, respectively.

While rotating the mold, the temperature was kept constant at 44 °C for 12 h, which is just below the solidification point of the Ti/camphene slurry. This allowed the nucleation and extensive growth of camphene crystals, while preserving the homogenous distribution of Ti walls made from the Ti particles. The frozen bodies were removed from the Al molds and isostatically pressed by cold isostatic pressing (CIP) at 200 MPa to enhance the packing of the Ti particles. The frozen Ti/camphene bodies were freeze-dried to remove the camphene crystals and sintered at 1300 °C for 2 h in a vacuum.

2.2.2 Characterization

The pore structures of the fabricated porous Ti scaffolds were characterized by scanning electron microscopy (FE-SEM, JSM- 6330, JEOL Techniques, Tokyo, Japan). The porosity was computed using the mass and volume of the samples in the following equation:

$$P = 100 \left(1 - \frac{m_S/V_S}{\rho_{Ti}} \right)$$

where P is the total porosity percentage, ρ_{Ti} is the theoretical density of the titanium and m_S/V_S is the measured density of the sample calculated using the mass (m_S) and volume (V_S). The average pore size was measured from the SEM images of the samples prepared by filling the porous Ti scaffolds with an epoxy resin (Spurrs epoxy Polysciences Inc., Warrington, PA). In

addition, the porous structure (e.g. porosity, pore size, and pore size distribution) was more closely examined using a micro-computed tomography scanner (micro-CT, Skyscan 1173, Skyscan, Kontich, Belgium).

The crystalline structure and chemical composition of the samples were analyzed by X-ray diffraction (XRD, M18XHF-SRA, MacScience Co., Yokohama, Japan) and energy dispersive spectroscopy (EDS) attached to the SEM, respectively. In addition, possible impurities, such as oxygen, hydrogen, carbon and nitrogen, were carefully examined using an elemental analyzer (EA1110, CE Instrument, Italy). During the analyzing procedure, 100 mg of the sample was oxidized by the dynamic flash combustion method and the resulting combustion gases were characterized using gas chromatography.

2.2.3 Mechanical properties

The compressive strengths of the porous Ti scaffolds with a diameter and height of 16 mm and 20 mm, respectively, were examined using a screw-driven load frame (Instron 5565, Instron Corp., Canton, MA, USA) at a crosshead speed of 5 mm/min. The stress and strain responses of the samples were monitored during the compressive strength tests. Five samples were tested to obtain the mean values and the standard deviation.

2.3 Results and discussion

2.3.1 Characterization

Figure 8 shows a schematic diagram of the process in which 3-

dimensionally interconnected large pores surrounded by Ti walls are created using dynamic freeze casting. A homogenous Ti/camphene slurry was first prepared by ball-milling at 55 °C for 30 min, transferred to an aluminum (Al) mold, then rotated continuously at 44 °C for 12 h which is close to the solidification point of the slurry. During this process, camphene crystals can nucleate and grow extensively until the slurry has completely solidified, while preserving the walls that are made of Ti particles, particularly due to freezing in rotation, as shown in Figure 9. The 3-dimensionally interconnected large pores can be created after removing the camphene crystals.

Figure 10 shows a typical optical image of the porous Ti scaffolds produced with various initial Ti contents (15, 20, and 25 vol%). No signs of sedimentation of the Ti particles were observed in any of the fabricated samples. This suggests that dynamic freeze casting (i.e., freezing in rotation) is quite useful for producing porous Ti scaffolds with a uniform pore structure, which is unobtainable by the conventional freeze casting, in which the relatively large Ti particles settle during solidification [68]. However, there is a limitation in the amount of initial Ti contents. It should be noted that the frozen bodies produced with the initial Ti contents of 5 and 10 vol% collapsed during the removal of the camphene crystals in the freeze drying process, because the strength of the green bodies decreased.

Figure 11 (A) show the micro-CT images of the porous Ti scaffolds produced by conventional freeze casting. The pore structure of the samples produced using conventional freeze casting has some directionality and irregular pores. On the other hand, the sample produced by dynamic freeze

casting exhibited nearly spherical pore structure, as shown in Figure 11 (B). This suggests that camphene crystals are likely to grow isostatically during the freezing process in rotation, which differs from the conventional freeze casting, in which camphene dendrites grow along the direction of heat conduction, creating elongated pores [75, 83].

Figure 12 (A)-(C) show SEM images of the porous Ti scaffolds produced with various initial Ti contents (15, 20, and 25 vol%). Regardless of the Ti content, all the fabricated samples showed spherical-like pores formed uniformly, which were created after removing the camphene crystals.

Figure 13 (A) shows typical SEM images of the Ti walls formed in the sample produced with an initial Ti content of 15 vol%. Regardless of the Ti content, all the fabricated samples showed well-densified Ti walls without noticeable pores and cracks. This was achieved by cold isotactic pressing (CIP), which could enhance the packing of the relatively large Ti particles, allowing the full densification of Ti walls even for a low Ti content of 15 vol%. On the other hand, the sample produced without the CIP process exhibited a number of relatively large pores because of the low packing density of Ti particles, as shown in Figure 13 (B).

The chemical compositions of the samples were characterized by XRD and EDS. The typical XRD pattern of the sintered sample with an initial Ti content of 15 vol% is shown in Figure 14. The sintered sample only showed peaks related with the crystalline Ti phase, suggesting that camphene has no influence on phase composition of the porous Ti. Figure 15 shows a typical EDS spectrum of the sample produced with an initial Ti content of 15 vol%. Strong peaks associated with Ti metal were observed without any

noticeable secondary elements. In addition, the possibility of impurities, such as oxygen, hydrogen, and carbon, were examined using an elemental analyzer, as summarized in Table 4. The oxygen content, originating mainly from the starting Ti particles, was much lower than the critical value which can deteriorate the ductility of Ti metal [67, 79]. This suggests that the dynamic freeze casting is a very promising method for the production of highly pure, porous Ti scaffolds with a very low oxygen content, which is attributed to the negligible chemical reaction between the Ti particles and camphene.

2.3.2 Mechanical properties

Table 5 lists the porosity and pore size of the fabricated samples produced with various initial Ti contents (15, 20, and 25 vol%). The porosity, which was computed by considering the mass and dimensions of the samples, decreased from 71 to 52% with an increase in Ti content from 15 to 25 vol%, whereas the pore size, which was estimated from the SEM images of the samples, decreased from 362 to 95 μm . This finding suggests that a lower Ti content can readily lead to larger pore size and higher porosity. In general, a higher porosity of bone scaffold can induce a faster bone ingrowth into the pores; however, it will inevitably cause a severe reduction in mechanical properties. Thus, the porosity and mechanical properties of the Ti scaffolds should be balanced properly to provide a favorable environment for bone ingrowth, while preserving their excellent structural integrity during the healing process. Furthermore, it is believed that the pore size of the samples can be increased by increasing the casting time for dynamic freeze casting

without sacrificing their porosity, since camphene crystals can overgrow continuously at 44 °C which is close to the solidification point of the Ti/camphene slurry [71, 72].

The pore size distributions of the samples produced with various initial Ti contents of (A) 15, (B) 20, and (C) 25 vol% were examined more closely using a micro-CT, as shown in Figure 16. All of the samples showed a narrow pore size distribution, suggesting that the pores were created as the replica of the camphene crystals that had grown during the freeze casting in rotation. However, the average pore size decreased from 340 to 96 μm with an increase in Ti content from 15 to 25 vol%. It should be noted that the pore size obtained in this study was much larger than that obtained by conventional freeze casting, because of the very slow solidification rate of the Ti/camphene slurry with the assistance of rotation. The porosities of the samples produced with various initial Ti contents of 15, 20, and 25 vol% were 73, 62, and 52%, respectively, which was in good agreement with those measured using the mass and dimensions of the samples.

The mechanical properties of the porous Ti scaffolds produced with various initial Ti contents (15, 20, and 25 vol%) were evaluated by compressive strength tests. Figure 17 shows the typical stress versus strain responses of the samples. Basically, all the fabricated samples exhibited the typical fracture behavior of the ductile metallic foams. In other words, three distinctive regions, namely, the linear elastic response, stress plateau, and densification regions were observed. This suggests that camphene is one of the most promising freezing vehicles for producing porous Ti scaffolds with good ductility.

Figure 18 present the compressive strengths and stiffness of the porous Ti scaffolds produced with various initial Ti contents (15, 20, and 25 vol%), respectively. The compressive strength increased considerably from 57 ± 4 to 183 ± 6 MPa with an increase in Ti content from 15 to 25 vol%, whereas the compressive stiffness increased remarkably from 1.3 ± 0.5 to 5.0 ± 0.8 GPa. These increases in compressive strength and stiffness were mainly attributed to a decrease in the porosity of the sample. On the other hand, it should be noted that these values are comparable to those of the cancellous bones, suggesting that the porous Ti scaffolds produced in this study will have useful applications as bone scaffolds [84].

It should be noted that it was possible to produce porous Ti scaffolds with a uniform porous structure using dynamic freeze casting that was newly developed in this study. This technique is very effective for producing the porous Ti samples with a cylindrical geometry; however, arbitrary complex 3-D geometries can be also manufactured using conventional computer numerical control (CNC) machines. This would enable the porous Ti scaffolds produced in this study to find very useful applications in bone tissue engineering.

2.4 Conclusions

Porous Ti scaffolds with a uniform porous structure were produced by dynamic freeze casting, in which Ti/camphene slurries with a range of initial Ti contents (15, 20, and 25 vol%) were frozen in rotation at 44 °C for 12 h. All the fabricated samples showed uniform spherical-like pores after removing the camphene crystals grown during freezing in rotation as well as

dense Ti walls after sintering at 1300 °C for 2 h in a vacuum. As the Ti content increased from 15 to 25 vol%, the porosity and pore size decreased from 71 to 52 vol% and from 362 to 95 μm , respectively. This led to a considerable increase in the compressive strength and stiffness from 57 ± 4 to 183 ± 6 MPa and from 1.3 ± 0.5 to 5.0 ± 0.8 GPa, respectively, as well as ductility, which was achieved by minimizing the level of oxygen contamination during the process.

Table 4. Oxygen, hydrogen, and carbon concentration of the porous Ti scaffold produced with an initial Ti content of 15 vol%.

Element	Oxygen	Hydrogen	Carbon
Concentration [ppm]	177	181	428

Table 5. Porosity and pore size of the porous Ti scaffolds produced with various initial Ti contents (15, 20, and 25 vol%).

Initial Solid Loading [vol %]	15	20	25
Porosity [vol %]	71	60	52
Pore Size [μm]	362	208	95

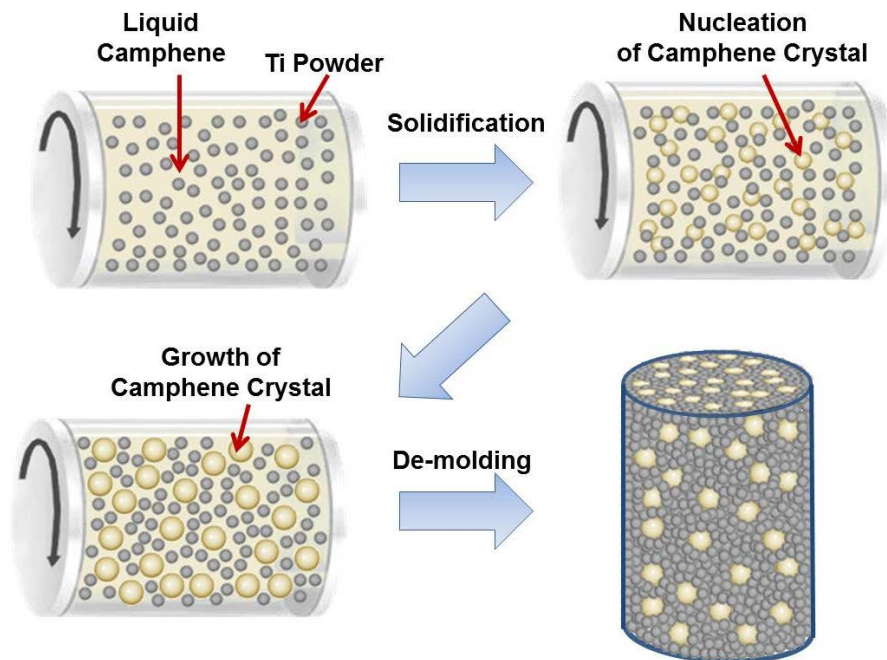


Figure 8. Schematic diagram illustrating the creation of large interconnected pores using dynamic freeze casting.

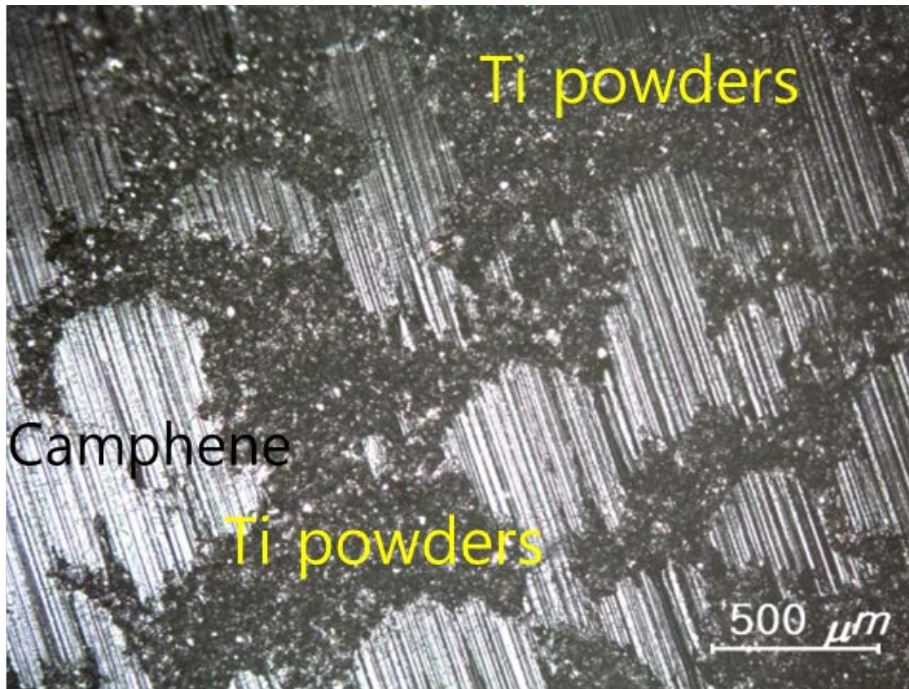


Figure 9. Optical image illustrating the green body of the dynamic freeze casting process.

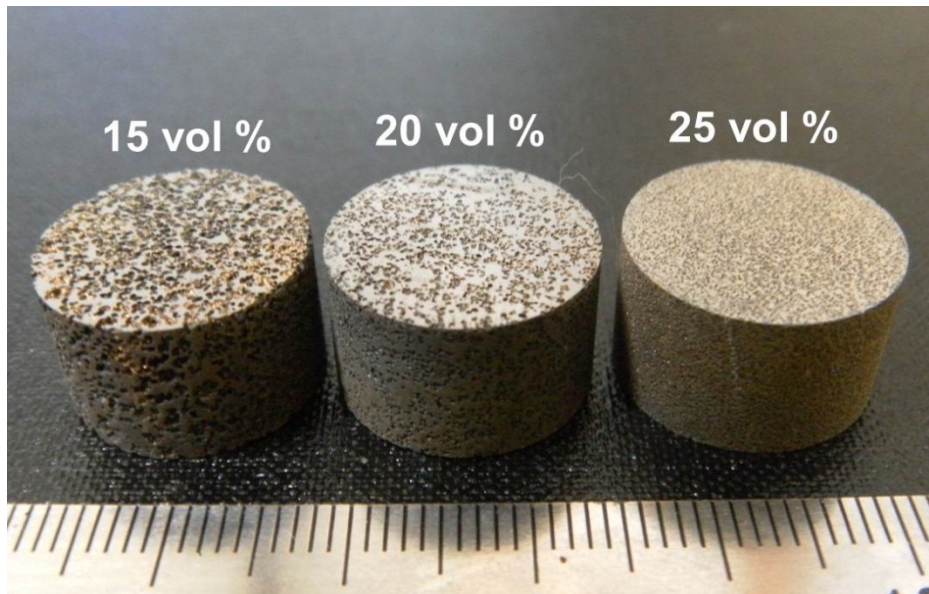


Figure 10. Typical optical image of the porous Ti scaffolds produced with various initial Ti contents (15, 20 and 25 vol%).

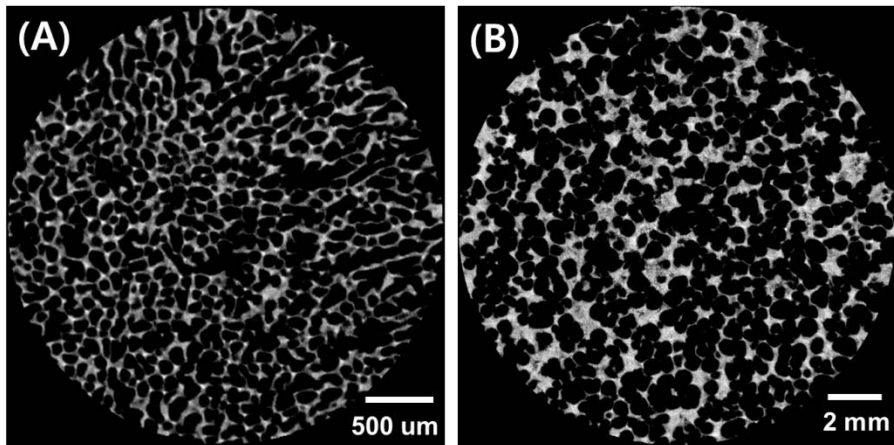


Figure 11. Micro-CT images of the porous Ti scaffolds produced with (A) conventional freeze casting, (B) dynamic freeze casting.

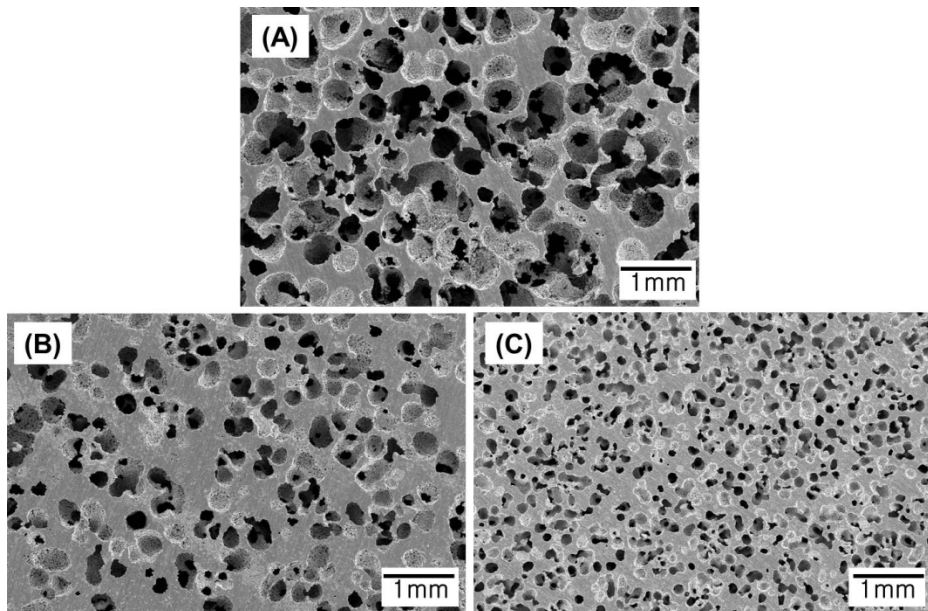


Figure 12. SEM images of the porous Ti scaffolds produced with various initial Ti contents of (A) 15, (B) 20, and (C) 25 vol%.

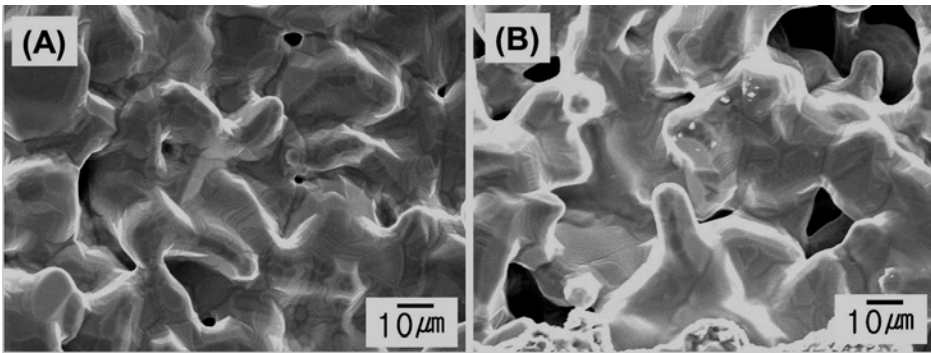


Figure 13. SEM images showing the Ti walls of the porous Ti scaffolds produced (A) with and (B) without the CIP process. (Initial Ti content = 15 vol%).

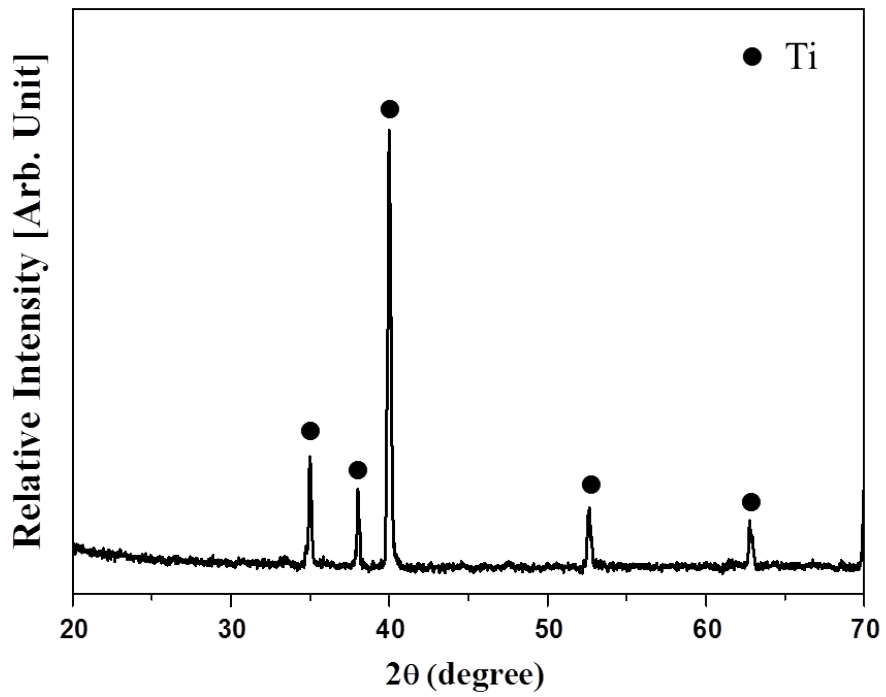


Figure 14. Typical X-ray diffraction patterns of the sintered sample with an initial Ti content of 15 vol%.

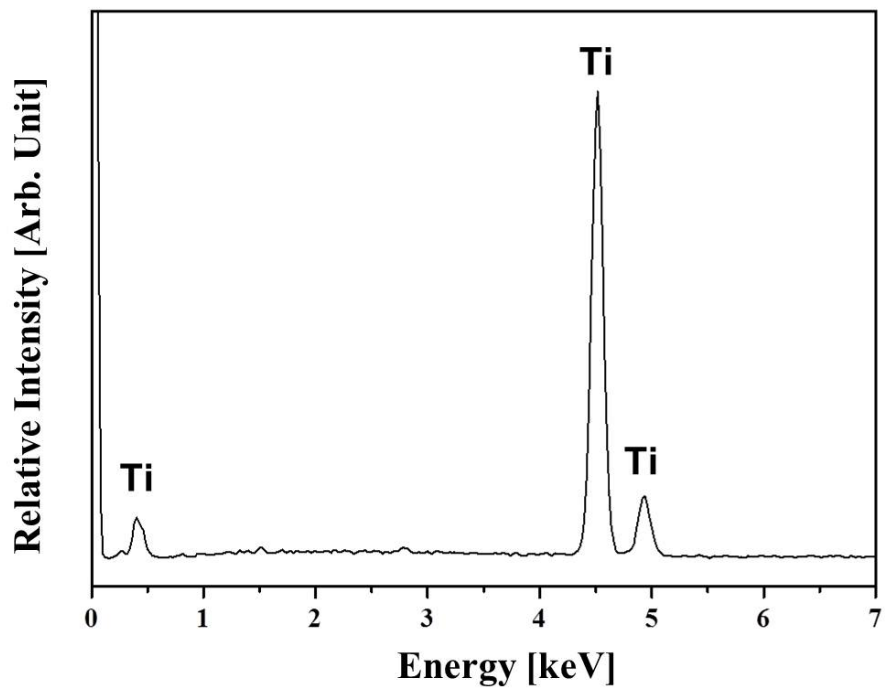


Figure 15. Typical EDS spectrum of the porous Ti scaffold produced with an initial Ti content of 15 vol%.

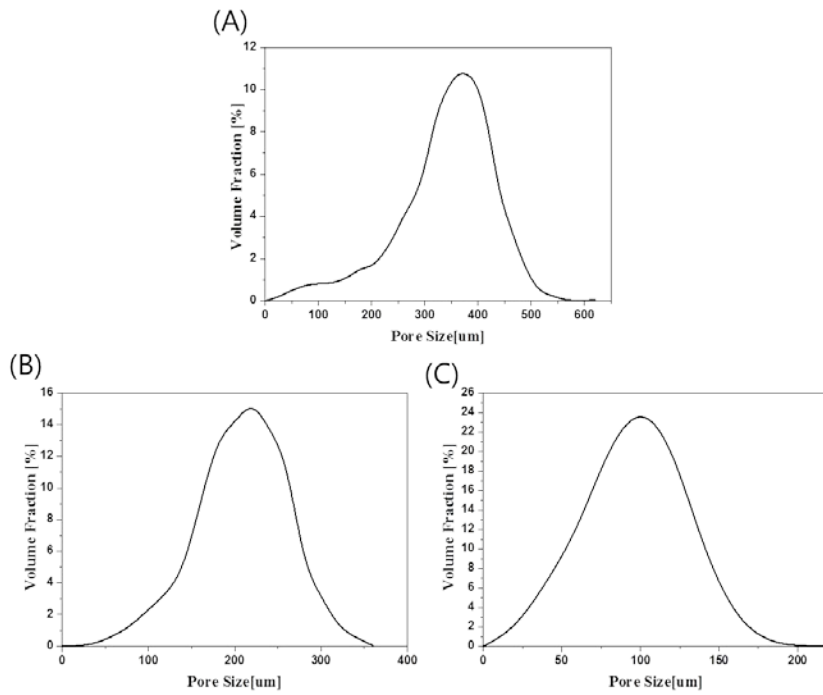


Figure 16. Pore size distributions for the porous Ti scaffolds produced with various initial Ti contents of (A) 15, (B) 20, and (C) 25 vol%.

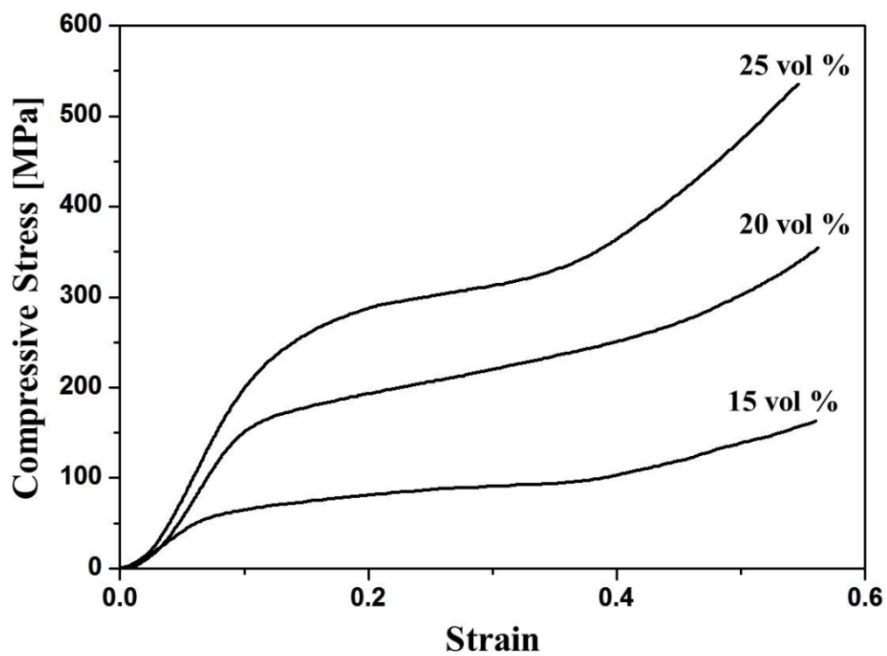


Figure 17. Typical compressive stress versus strain responses of the porous Ti scaffolds produced with various initial Ti contents (15, 20, and 25 vol%).

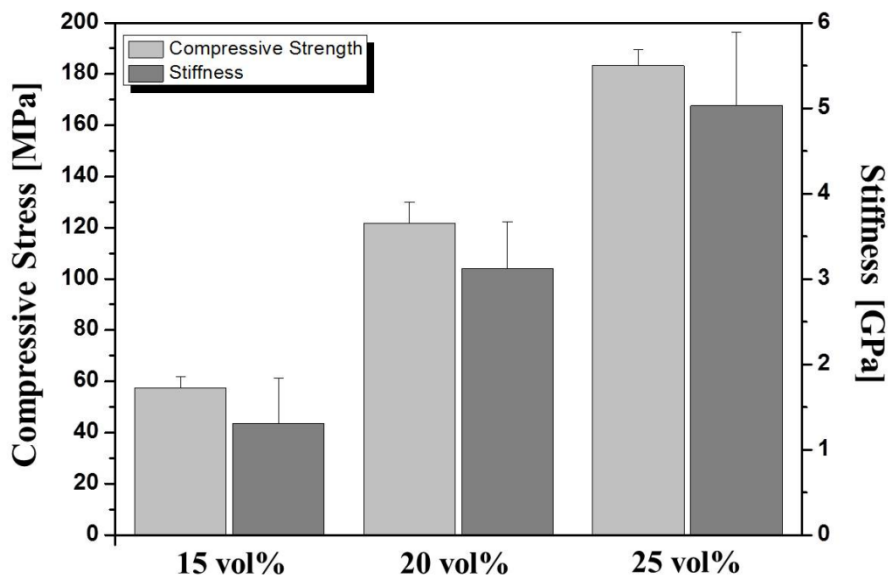


Figure 18. Compressive strength and stiffness of the porous Ti scaffolds as a function of the initial Ti content.

Chapter 3.
Sustained Release of BMP-2 from
Densified Titanium Scaffold

3.1 Introduction

Many researchers are focusing on finding ways to fabricate a material that can accelerate bone growth and regeneration while providing structural support and in dental and orthopedic implants. Implants are considered osteoinductive when growth factors, such as bone morphogenetic proteins (BMPs) are incorporated. BMPs have been widely used to accelerate the healing process of bone defects and are also used in medical and dental implants [85, 86]. They regulate various cellular activities by stimulating and inhibiting the cellular behaviors which are influenced by cell type, differentiation stage, dose, and exposure time. BMP-2 and BMP-7 are previously reported to induce bone formation in both heterotopic and orthotopic sites [87-91]. Therefore, many studies have incorporated BMP-2 in implants to stimulate and augment bone formation more quickly.

The release behavior of implant materials loaded with bioactive substances is highly dependent on the carrier. The time at which the release of BMP-2 occurs and the amount that is released are critical factors in a delivery system [86, 92-95]. An efficient carrier is one that can sustain the release of the bioactive molecules for a prolonged time since the carrier can undergo a rapid diffusion when exposed in physiological environment [34, 96]. Various materials have been proposed and investigated for use as BMP carriers which include synthetic polymers, collagen, calcium phosphate, and titanium [34, 96-99]. Titanium is often times the common choice of material when it comes to dental and orthopedic implant materials due to their excellent biocompatibility and mechanical properties. However, previously

studied titanium implants that have tried to improve the osteoconductivity are limited to manipulating the surface properties or coating the materials with a layer of calcium phosphate for loading BMP-2 [100-104]. Therefore, the development of a carrier system that is capable of a sustained and controlled release of biologically active BMP-2 over an extended time period is a goal that many researchers are trying to meet to devise an ideal growth factor releasing system [105-107].

It is expected that the titanium implants containing some amounts of BMP-2 which can be released continuously would enhance the bone formation at the implant surface and promote faster bone regeneration at the injured site. We hypothesized that the long-term release of growth factor will promote faster bone generation which will be reflected in *in vitro* and *in vivo* tests.

In this study, the bone regeneration properties as well as the release behavior of BMP-2-embedded densified Ti scaffolds were investigated. Porous Ti scaffolds were soaked in a solution containing BMP-2 in a vacuum state and was densified to control the release rate of BMP-2. BMP-2-embedded densified titanium scaffolds were explored for potential use as a novel growth factor releasing material. The mechanical property of BMP-2 embedded densified Ti scaffolds was evaluated with a tensile test, and the biocompatibility and the effectiveness of the embedded BMP-2 were characterized by *in vitro* and *in vivo* tests.

3.2 Experimental Procedure

3.2.1 Material Preparation

Porous titanium scaffolds with various porosities were used as the growth-factor carriers. The average pore size and porosity of the scaffolds used in this experiment are shown in Table 6. The prepared porous titanium samples were disc-shaped. Before use, all samples were sterilized in an autoclave for 15 min at 121 °C. Following the sterilization, the scaffolds were immersed in GFP or BMP-2 solution. Immersed specimens were put into a vacuum desiccator connected to a rotary pump for 10 min, incubated overnight at room temperature (RT), washed with DPBS twice and dried. GFP or BMP-2 loaded porous Ti discs were then uniaxially pressed in a mold. The densified samples were washed with DPBS and allowed to dry at RT.

3.2.2 Characterization

The structures of the fabricated Ti scaffolds were characterized by scanning electron microscopy (FE-SEM, JSM- 6330, JEOL Techniques, Tokyo, Japan). The pore size was measured and averaged from the SEM images of the samples prepared by filling the porous Ti scaffolds with an epoxy resin (Spurrs epoxy Polysciences Inc., Warrington, PA). The porosity was computed using the mass and dimensions of the samples in the following equation

$$P = 100 \left(1 - \frac{m_S/V_S}{\rho_{Ti}} \right)$$

P is the total porosity percentage, ρ_{Ti} is the theoretical density of the titanium and m_S/V_S is the measured density of the sample calculated using the mass (m_S) and volume (V_S). In addition, micro-computed tomography scanner (micro-CT,

Skyscan 1173, Skyscan, Kontich, Belgium) was used to further examine the structures of the scaffolds.

3.2.3 Mechanical properties

The mechanical properties of the densified titanium of various initial porosities were analyzed using Instron 5565 system (Instron, USA) with a cross-head speed of 5 mm/min. The samples used for the mechanical test were prepared by preparing densified titanium and obtaining dog bone shaped specimens through electrical discharging machining. The tensile samples were 3 mm wide, 20 mm long and 2 mm thick. The tensile strengths of the samples were obtained from the stress–strain curves. The number of specimens tested for each composition was five.

3.2.4 *In vitro* tests

GFP release

The concentration of GFP solution was 100 µg/ml for the *in vitro* release test. The as-received Ti, porous Ti specimens were immersed into the prepared GFP solution. Immersed specimens were put into a vacuum desiccator connected to a rotary pump for 10 min, incubated overnight at 4 °C and washed with DPBS twice. The GFP loaded Ti scaffolds (Φ 16 mm *2 mm) were immersed in 5 ml of PBS at 37 °C and pH 7.4 for 112 days. The solutions were suctioned and replenished daily for the first week and weekly for the rest of the experiment. The post-release surface fluorescence was observed for 0, 14, 28, 56 and 112 days following immersion with confocal laser scanning spectroscopy (CLSM).

BMP release

Similar method as presented above for the GFP release was used to characterize BMP release. The BMP-2 loaded Ti scaffolds (Φ 16 mm *2 mm) were immersed in 5 ml of PBS for 140 days. The solutions were exchanged daily for the first week and weekly for the rest of the experiment. The released BMP-2 amounts were measured with UV spectroscopy (ICP-AES, Optima-4300 DV, USA) at 220 nm. A calibration curve was prepared by measuring the optical absorbance of BMP-2 in PBS with various concentrations in the range of 0.010–10 $\mu\text{g/ml}$. The linear relationship between BMP-2 concentration and the absorbance was used to quantify BMP release. Each absorbance value was directly converted to the amount of BMP-2 released using the standard curve. The relative amounts of BMP-2 released were normalized to the initially loaded amounts of the titanium scaffolds ($n = 5$). After evaluating the release behavior, the PBS solutions containing the released BMP-2 were collected at 2, 4, 6, and 8 weeks into release and were used in cell tests to analyze the functionality of the released BMP-2 from the samples.

Cellular responses

The concentration of BMP-2 solution was 100 ng/ml for the *in vitro* cell test. The *in vitro* cellular responses of the BMP-2-embedded densified Ti were assessed using MC3T3-E1 cells and the results were compared with those obtained using the as-received Ti and as-received Ti adsorbed with BMP-2. The biological activities of the released BMP-2 were evaluated

using the solution containing the released BMP-2 at various times. The collected solutions were all diluted to 10 ng/ml and were supplemented to the culturing medium to analyze their effects on cell proliferation and differentiation. A negative control was set as the culturing medium with no BMP-2 solution added, and a positive control was set as the culturing medium directly supplemented with fresh BMP-2. The cells were seeded onto the specimens at densities of 5×10^4 , 1×10^4 and 2.5×10^3 cells/mL for the cell attachment, proliferation and differentiation tests, respectively. The cells were cultured in a humidified incubator with 5% CO₂ at 37 °C. Alpha-minimum essential medium (a-MEM, Welgene Co., Ltd., Korea) that was supplemented with 2% fetal bovine serum (FBS) and 1% penicillin–streptomycin was used as the culturing medium, and 10 mM β-GP and 50 ug/mL ascorbic acid were added for the alkaline phosphatase (ALP) test. For the initial cell adhesion test, the cells were cultured for 3 h and fixed in 4% paraformaldehyde in PBS for 10 min, rinsed in PBS, permeabilized with 0.1% Trion X-100 in PBS for 5 min, and rinsed again in PBS. In order to observe the cell morphology, phalloidin (Alexa Fluor® 555 phalloidin, Invitrogen, USA) was used to stain the cells for 20 min and the nuclei were stained with 4',6-diamidino-2-phenylindole (DAPI; ProLong® Gold antifade reagent with DAPI, Invitrogen, USA) for 5 min. The stained specimens were mounted on cover slides and the cell attachment morphology was observed using CLSM (FluoView FV1000, Olympus, Japan). To characterize the cell viability, cells were cultured for 3 and 5 days and an MTS assay (CellTiter 96 Aqueous One Solution, Promega, USA) was used to study the proliferation. The absorbance measurements that were taken at 490 nm using a micro-reader

(Biorad, Model 550, USA) is directly proportional to the number of living cells; therefore the absorbance was used to estimate the amount of living cells. The cell differentiation was studied by measuring the alkaline phosphatase (ALP) activity on day 10. The alkaline phosphate (ALP) activity, which indicates the degree of cell differentiation, was measured as an early indicator of the osteoblastic phenotype maintenance using p-nitrophenyl phosphatase (pNPP, Sigma-Aldrich, UK). The conversion of pNPP to p-nitrophenol (pNP) in the presence of ALP results in a color change. This colorimetric change can be used to predict which the ALP activity since the rate of pNP production is proportional to the ALP activity. A micro-plate reader was used to determine the absorbance at 405 nm. The ALP activity was calculated against a standard curve that was obtained using bovine serum albumin with a concentration ranging from 0.2 to 1.2 mg/mL. The MTS assay and ALP activity test were performed on three samples (n = 3) for each condition. The statistical analysis was performed via one-way analysis of variance (ANOVA), with the level of significance set at $p < 0.05$.

3.2.5 *In vivo* tests

Experimental design

The concentrations of BMP-2 solution used for the *in vivo* test was 700 µg/ml. BMP-2-embedded densified Ti was used as the experimental sample and samples as-received Ti and BMP-2-adsorbed as-received Ti were used as control samples. The implant was a ring structure measuring 12 mm in diameter, 2 mm in thickness, with a 8 mm diameter hole. Six discs per each group were implanted in rabbit calvarias. Figure 19 (A) and (B) shows

the rings and screws used and the surgical site following the placement of the implants.

Implantation

The animal test was conducted using nine New Zealand white male rabbits (12 weeks old, average weight 3 kg). The animals were weighed at the beginning and at the end of the experiment. All rabbits had a normal diet and were cared under the same conditions. Each animal had two implanted ring implants, one on the upper part and the other on the lower part of the calvaria. With this condition, the three groups of ring implants were distributed among the 9 animals according to a systematic protocol. The surgical sites were shaved and the skin was treated with a surgical prep solution containing 10% povidone-iodine (Betadine). Surgery was performed under conditions of general anesthesia with 0.1 cc of 2% Xylazine HCl (Rompun, Bayer Korea, Korea), 0.2 cc of Tiletamine HCl (Zoletil, Virbac lab, France) and Lidocaine (Yuhan Corporation, Korea). An incision of approximately 4 cm was made at the site of implant placement. A 12 mm diameter trephine bur was used to make two holes through the calvaria on each side of the median calvarial suture and the 12 mm diameter×2 mm ring implants were placed in the holes. The wounds were sutured using Surgisorb (Samyang Ltd, Korea). Gentamicin (0.1 mg/kg SQ) was injected immediately following the operation, then every 24 h to 1 day for 3 days. Animals were monitored daily for any adverse reaction. 6 weeks following implant placement, the animals were sacrificed by asphyxiation with carbon dioxide. The rabbit calvarias were harvested and the tissues

from the implant sites were collected and fixed in 10% neutral-buffered formalin.

Quantitative micro-computed tomography evaluation

Following the fixation, the bone volume of new supracalvarial mineralized tissue was analyzed using computed microtomography with the following parameters: 0.25 mm brass filter, 180° rotation, 3-frames averaging, 0.2° rotation step, 12 µm resolution, 130 kV voltage, and 60 µA current (Skyscan 1173 X-ray Micro-tomography System, Skyscan, Kontich, Belgium). The acquired images were processed using a commercial program and the implant morphology and the bone tissues were 3-dimensionally observed using Data viewer (Skyscan, Kontich, Belgium). The gray-scale images were obtained with a fixed threshold to extract the Ti away from the new bone and the new bone volume was measured using CTAn (Skyscan, Kontich, Belgium) analysis software. The statistical analysis was performed via one-way analysis of variance (ANOVA), with the level of significance set at $p < 0.05$.

3.3. Results and Discussion

3.3.1 Characterization

The internal microstructures of the densified samples were studied. The effect of applying different pressures on the porous scaffold was explored by condensing the samples in a mold with uniaxial pressure and studying the resultant microstructures. As shown in Figure 20, the heights of the samples decreased with increasing pressures. The microstructures of the

densified samples observed with SEM are shown in Figure 21. With an increase in pressure, porosity and pore size decreased. The ductility of titanium enabled the densification of the porous sample to be successful without crushing or fracturing. With 2000 MPa of applied pressure on the scaffolds, the porosity was 7% and no significant change to the porosity was made with higher pressure. The changes of the porous structure due to various pressures are shown in Table 7. Micro-CT images of the densified samples were observed as well (Figure 22). The microstructure shows that densification occurred uniformly throughout the scaffolds.

3.3.2 Mechanical properties

The tensile properties of the densified Ti scaffolds with various initial porosities are shown in Figure 23. Scaffolds with various porosities were densified and machined to make the tensile test samples. The prepared samples were pulled perpendicular to the direction of applied pressure on the scaffolds for the densification process. Commercially available Ti grade 2 was machined and tested as well to compare with the fabricated and densified titanium. As the initial porosity decreased from 71% to 43%, the tensile strength increased from 44 to 164 MPa. As porosity increases, the struts that support the scaffold becomes thinner and scaffolds become weaker than grade 2 Ti even after densification. Another possible factor for lower strength is that the densified materials are not 100% dense and the presence of pores can weaken the material. However, the mechanical properties of the densified scaffolds are similar to the mechanical properties of the human cortical bone [59]. Therefore, the exploration of the novel

materials is worthy of further study for potential use in the dental and orthopedic field.

3.3.3 *In vitro* tests

GFP release

Before testing with BMP-2, green fluorescent protein (GFP) was used to perform a release test to verify the potentials of using the densified Ti scaffold as growth factor carriers. GFP was embedded into Ti and its release behavior in PBS was monitored using CLSM. When the same concentration of GFP was used for the as-received Ti, porous Ti and densified Ti, the intensities of the green fluorescence were about the same in the images taken immediately after loading GFP as shown in Figure 24. However, after 14 days of immersion in PBS, the green fluorescence observed from the porous Ti was significantly lower than that of the signals observed from the GFP-embedded densified Ti. The green fluorescence of the bare Ti was not detected. After 28 days of immersion, there was still a trace of green fluorescence from the GFP-embedded densified Ti, while none was observed from the as-received Ti and porous Ti. Even after 112 days, the green fluorescence on the narrow pores was detected from the GFP-embedded densified Ti. This suggests that GFP was released continuously from the GFP-embedded densified Ti at a very slow rate.

BMP-2 release

The sustained growth factor release behavior was evaluated by monitoring the cumulative amount of the released BMP-2. Figure 25 shows

the optical images of the samples. To study the growth-factor loading capacity of the scaffolds, scaffolds with various porosities of 71, 60, 52, and 43% were prepared. In order to match the densified heights of the samples, the prepared scaffolds with different initial heights (dependent on the porosities) were pressed to a final height of 2 mm. The same concentration of BMP-2 was used for each sample. Figure 26 shows the cumulative amount of released BMP-2 from each of the specimen. P and D stand for porous and densified, respectively. All of the BMP-2 was released from as-received Ti within 1 day. This result indicates that the surface of as-received Ti is not suitable for growth factor carrier. As initial porosity of Ti increases, the quantity of the loaded BMP-2 was increased. Although the same concentration of BMP-2 was used for all samples, the cumulative amounts of BMP-2 released from the P71 and D71 samples were about 52 μg , while the cumulative amounts of BMP-2 released from the P43 and D43 samples were about 16 μg . It should be noted that the amounts of BMP-2 loading can be modulated by varying the initial porosity of Ti.

BMP-2 was released rapidly from the porous Ti during the initial 1 week and then slowly thereafter. After 2 weeks, very small amounts of BMP-2 were released. On the other hand, the release of BMP-2 from the BMP-2 embedded Ti was relatively steady in which considerable amounts of BMP-2 were released even after 20 weeks. It should be noted that BMP-2 embedded Ti remarkably reduced the initial burst effect when compared to the porous Ti.

The difference in the release behavior of drugs resulted from different release kinetics. Figure 27 shows schematic diagrams of the

mechanism of sustained release from dense titanium scaffold. When BMP-2 is loaded and densified, the BMP-2 is embedded in the titanium scaffold. Once the sample is soaked in PBS, BMP-2 is diffused at the surface and from the interior as well. However, with the porous scaffolds that are not densified, PBS easily infiltrates the interior of the scaffold through the large pores and BMP-2 is quickly released. However, with the densification process, the porosity of the scaffold drops to approximately 7% and the pore size is about 10 μm . The release rate of the BMP-2 from the densified titanium is consequently much slower since embedded BMP-2 is released through a very narrow pathway. By applying this concept, more BMP-2 can be embedded in the scaffold for sustained and controlled release of BMP-2 from the densified scaffolds.

The relationship between the degree of densification and the release behavior of BMP-2 was also evaluated by the BMP-2 release profile. Figure 28 shows the optical images of the samples. Porous Ti with initial porosity of 52% was pressed, and the Ti scaffolds with various porosities (52%, 43%, 24% and 7%) were fabricated. The cumulative amounts of BMP-2 released from the Ti scaffolds were measured as a function of time as shown in Figure 29. The cumulative amounts of BMP-2 were almost the same because BMP-2 was loaded into the samples before densification. However, the release rate of each sample decreased as the degree of densification increased. This suggests that the release rate is determined by pore size which can be altered with the degree of densification.

Cellular responses

Cell Attachment

The *in vitro* cellular responses of the BMP-2 embedded Ti were examined in terms of the initial attachment, proliferation and differentiation levels of pre-osteoblast cells. Samples with initial porosity of 50% were chosen for *in vitro* tests which showed adequate strength and release profile from the tensile and release tests. For controls, as-received Ti and BMP-2-adsorbed as-received Ti were used. Figure 30 shows the CLSM images of the MC3T3-E1 cells adhering to the surface of Ti scaffolds after culturing for 3 h on (A) as-received Ti, (B) BMP-2- adsorbed as-received Ti and (C) BMP-2-embedded densified Ti. The red and blue colors in the images represent f-actin and nucleus of the cell, respectively. For all the specimens, similar amounts of cells attached on the surface and spread well. On as-received Ti, the cells adhered well, as shown in Figure 30 (A). The cells adhered and spread even better on BMP-2-embedded densified Ti (Figure 30 (C)). As shown in Figure 30 (B), the cells adhered well on the adsorbed surface of as-received Ti, but not as well as those on the BMP-2-embedded densified Ti.

MTS Assay

The cell viability on different substrates was characterized with MTS assay on day 3 and day 5 of culturing as shown in Figure 31. The cell viability of all the samples increased from day 3 to day 5. However, there were no significant differences among the proliferation levels of each specimen cultured for 3 days ($p > 0.05$). These results indicate that all specimens offered favorable environment for the cells to attach and

proliferate.

However, after culturing 5 days, it is worth noting that the cells that adhered to BMP-2-embedded densified Ti showed significantly higher cell viability than those of as-received Ti and BMP-2-adsorbed as-received Ti ($p < 0.05$). The result indicates that sufficient amounts of BMP-2 from BMP-2-embedded densified Ti improved the cytocompatibility of Ti scaffolds.

Moreover, the results of the cell viability test performed with cells supplemented with the released BMP-2 solutions in the culturing medium show similar trends in the amount of proliferation of cells. No significant differences among the samples were observed in the results obtained. However, the level of viability from day 5 samples was more than twice the level of viability from day 3. No apparent cytotoxicity was observed and all specimens provided favorable environment for cell growth and proliferation.

ALP Assay

The level of initial cell differentiation evaluated by the ALP activities of the MC3T3-E1 cells cultured for 10 days on as-received Ti, BMP-2- adsorbed as-received Ti and BMP-2-embedded densified Ti are shown in Figure 32. The ALP activity of the cells on BMP-2-embedded densified Ti was significantly higher than that on the as-received Ti and BMP-2- adsorbed as-received Ti ($p < 0.05$). When BMP-2 was adsorbed on the surface of as-received Ti, both the cell viability and ALP activity were almost the same compared to those of the as-received Ti. This indicates that insufficient amount of BMP-2 were released from the Ti adsorbed with BMP-2 to show a significant difference. In contrast, the ALP activity of the

cells on BMP-2-embedded densified Ti was high because sufficient amount of BMP-2 stimulated cells continuously.

From the *in vitro* cell test results, it can be interpreted that BMP-2 released from BMP-2-embedded densified Ti was internalized by osteoblast cells and in turn promoted pre-osteoblast cell differentiation and proliferation. Many research demonstrated that BMP-2 plays a critical role in up-regulating transient PI3 kinase and Akt kinase which in turn shows enhanced cell viability, proliferation and migration [108-110].

The differentiation levels of the cells that were cultured with the BMP solution obtained on week 2, 4, 6 and 8 showed significantly higher levels of ALP activity when compared to that of the cells cultured in a medium without any BMP-2 supplements (negative control). The BMP-2 supplemented with fresh BMP-2 directly into the medium (positive control) promoted cell differentiation and showed higher levels of ALP activity when compared to the negative control. The samples that were cultured with the solutions containing BMP-2 released on week 2, 4, 6 and 8 showed a slightly decreasing trend in ALP activities, however all samples showed increased ALP activity when compared to that of the negative control. The results show that BMP-2 from the densified samples is bioactive even after 8 weeks of release and were able to induce differentiation of cells. The concentration of the released BMP-2 from week 10 was 60 ng/ml. The amount of released BMP-2 was minimal thus no further cell tests were performed with the solutions obtained from week 10 and onward.

3.3.4 *In vivo* tests

All animals showed sufficient amount healing at the surgical site and no infections were observed. Furthermore, all animals were in good health conditions with no noticeable change in body weight and diet. At the time of sample retrieval, the ring implants were very stable in the defect site and were covered by a thick layer of new soft tissues that were formed following the operation (Figure 19 (C)). Micro-CT images of the calvaria region with the implants and the surrounding tissues in the calvaria were obtained and used to measure the extent of new bone generation around the three implanted samples. Representative micro-CT images are shown in Figure 35 and 36. There were no new bone growth evident around any of the as-received Ti implants on the 2-D reconstructed micro-CT images; however, little amounts of new bone were observed around the BMP-2-adsorbed as-received Ti implants, particularly the BMP-2-embedded densified Ti implant (Figure 35).

In addition, to compare the new bone formation more quantitatively, 3-D reconstructed micro-CT images were utilized as shown in Figure 36. The as-received sample shows no bone formation in the interior of the ring. In addition, minimal bone cell interaction is observed on the outer region between the implant and the defect wall (Figure 36 (A)). In Figure 36 (B), the BMP-2-adsorbed as-received Ti sample showed enhanced bone formation on the outer surface of the implant and minimal amounts of new bone was generated in the inner region. In contrast, a substantial amount of bone growth was observed for the BMP-2-embedded densified Ti implant as shown in Figure 36 (C). The bone formation on the outer region of the sample as well as the interior region showed significant improvement when compared to that

of the other two samples.

A quantitative analysis of the new bone generation was performed as shown in Figure 37. The volume of the newly formed bone was quantified by subdividing the regions into interior and total space as shown in Figure 37 (A). The as-received Ti sample had very minimal new bone formation in the interior region and had the lowest amount of the overall new bone volume ($0.8 \pm 0.1 \text{ mm}^3$) when compared to the other two samples (2.6 ± 0.7 and $9.6 \pm 3.0 \text{ mm}^3$ for BMP-2-adsorbed as-received Ti and the BMP-2-embedded densified Ti respectively) (Figure 37 (B)). Amounts of the new bone formation of BMP-2-adsorbed as-received Ti showed increased new bone volume when compared to the as-received Ti suggesting that the adsorbed BMP-2 of the samples had a stimulatory effect on the osteoblast cells. The BMP-2-embedded densified Ti samples showed significantly larger amounts of new bone formation when compared to the other two ($p < 0.05$). The significantly high bone growth of the densified sample could be explained with BMP-2 promoting quicker regeneration and mineralization of the bone tissue around the implant. The new bone volume of the total space increased from as-received to the adsorbed sample (30.2 ± 10.0 and $36.7 \pm 10.0 \text{ mm}^3$ respectively). Moreover, BMP-2-embedded sample showed the highest amount of volume ($50.7 \pm 13.0 \text{ mm}^3$). However, the results did not show statistically significant differences among the samples. These results suggests that that BMP-2-embeded densified Ti implant can sustain BMP-2 release for a prolonged time and that it is a promising material that can be used as potential growth factor carrying implant material.

Designing a scaffold that can deliver BMP-2 to promote quicker

bone regeneration needs to consider the following requirements: (a) supplying of BMP-2 in a biologically relevant manner, (b) providing osteogenic stimulations through direct biochemical/ biomechanical signaling, (c) retaining a porous, osteoconductive surface that supports cell attachment and cell infiltration, and (d) maintaining sufficient mechanical strength for the surgical application. Various materials such as poly-DL-lactic acid scaffolds, nanofibrous chitosan membrane, polylactide/glycolide polymers, and nanohydroxyapatite/ collagen/poly-L-lactic acid scaffolds have been used as BMP carriers [111-114]. In previous studies, BMPs have been incorporated into implants in various ways: infused in titanium sponges, covalently bonded through chromosulfuric acid treatment, impregnated in hydroxyapatite plasma-splayed around implants, and soaked in polylactic acid membranes [115-118].

Titanium (Ti) is a commonly utilized material in many medical device applications and many researchers have focused on enhancing its surfaces properties to improve its performance in medical applications. Recent studies that focus on the surface modification of grafting materials for inducing rapid bone ingrowth have utilized stimulatory molecules, which includes peptides, proteins, and growth factors on the surface that enables quicker and more stable cell colonization [119, 120]. Considerable effort has been devoted to ensure the stable localization of bioactive molecules using either a physical adsorption or chemical crosslinking methods [121, 122]. Physical adsorption has limitations since using soluble growth factor may not be sufficient for long-term implantation due to protein desorption and/or exchange with physiologic fluid contact.

Therefore, in this work, porous titanium was fabricated, loaded with BMP-2 into the pores, and densified for sustained release of BMP-2. The mechanical properties, *in vitro* and *in vivo* test results presented in this study suggest that that BMP-2-embedded densified Ti may have potential for future dental and orthopedic materials.

3.4. Conclusions

The growth factor carrier with a sustained release was fabricated by densifying porous Ti scaffolds after loading BMP-2. Porosity and pore size of densified Ti decreased with an increase in pressure without any cracks and defects. The tensile strengths of the densified scaffolds range from 44 to 164 MPa. The release of BMP-2 from the BMP-2-embedded densified Ti was relatively steady in which considerable amounts of BMP-2 were released even after 20 weeks. The *in vitro* cell tests revealed that the BMP-2-embedded densified Ti scaffold significantly enhanced the cellular responses and the bioactivity. Micro-CT analysis showed that BMP-2-embedded densified Ti significantly promoted the bone repair in cavity of rabbit calvarias. These results suggest that that BMP-2-embedded densified Ti have potentials for future dental and orthopedic materials.

Table 6. Porosity and pore size of the Ti scaffolds that were used in this experiment.

Name	P71	P60	P52	P43
Porosity [%]	71	60	52	43
Pore size [μm]	362	208	95	90

Table 7. Porosity and pore size of the densified Ti scaffolds with various pressure conditions..

Pressure [MPa]	0	250	500	1000	1500	2000
Porosity [%]	71	56	33	19	13	7
Pore size [μm]	362	265	149	37	19	13

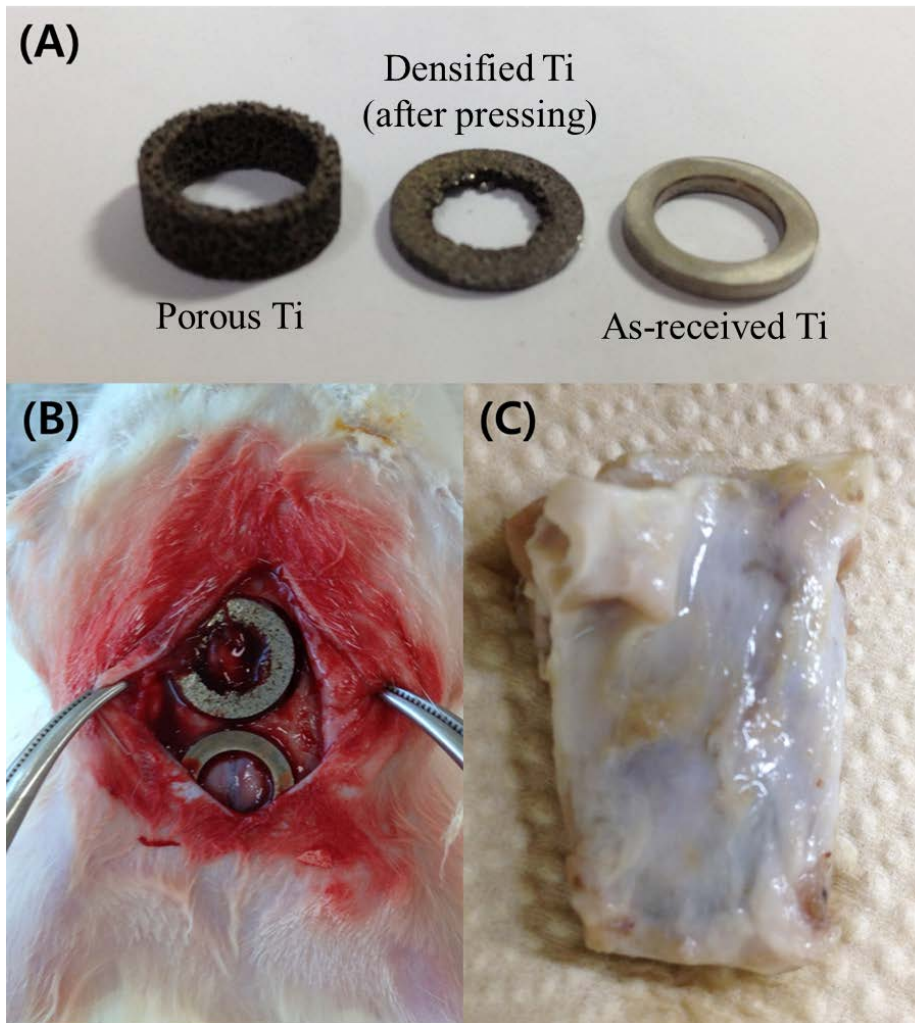


Figure 19. Rabbit calvarial implants and their surgical placements. (A) Ring type porous Ti implant, densified titanium after pressing and as-received Ti samples (B) Two implants were placed side by side into the calvaria of each rabbit randomly. (C) Representative rabbit calvaria images retrieved 6 weeks after implantation

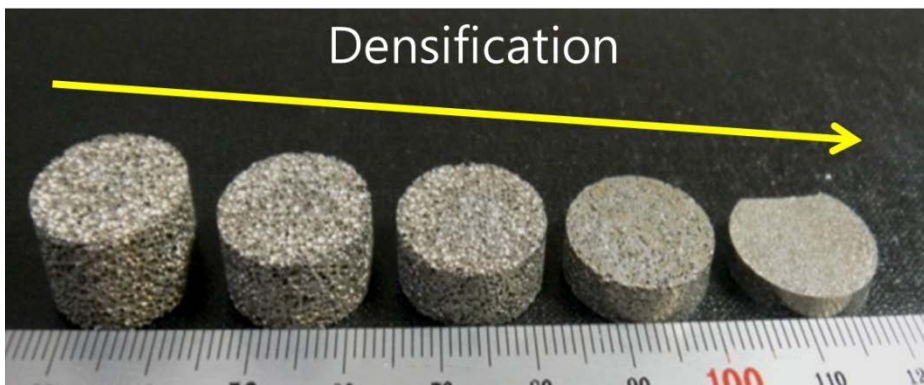


Figure 20. Optical image of the Ti scaffolds with increasing uniaxial pressings.

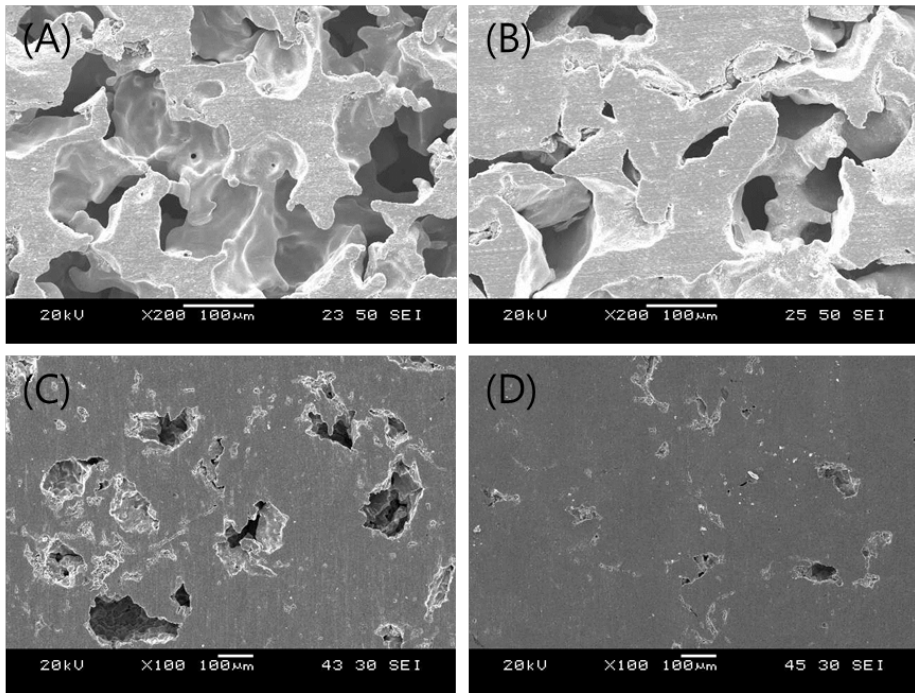


Figure 21. SEM images of the Ti scaffolds with increasing uniaxial pressings; (A) w/o pressing, (B) 500 MPa, (C) 1000 MPa and (D) 2000 MPa.

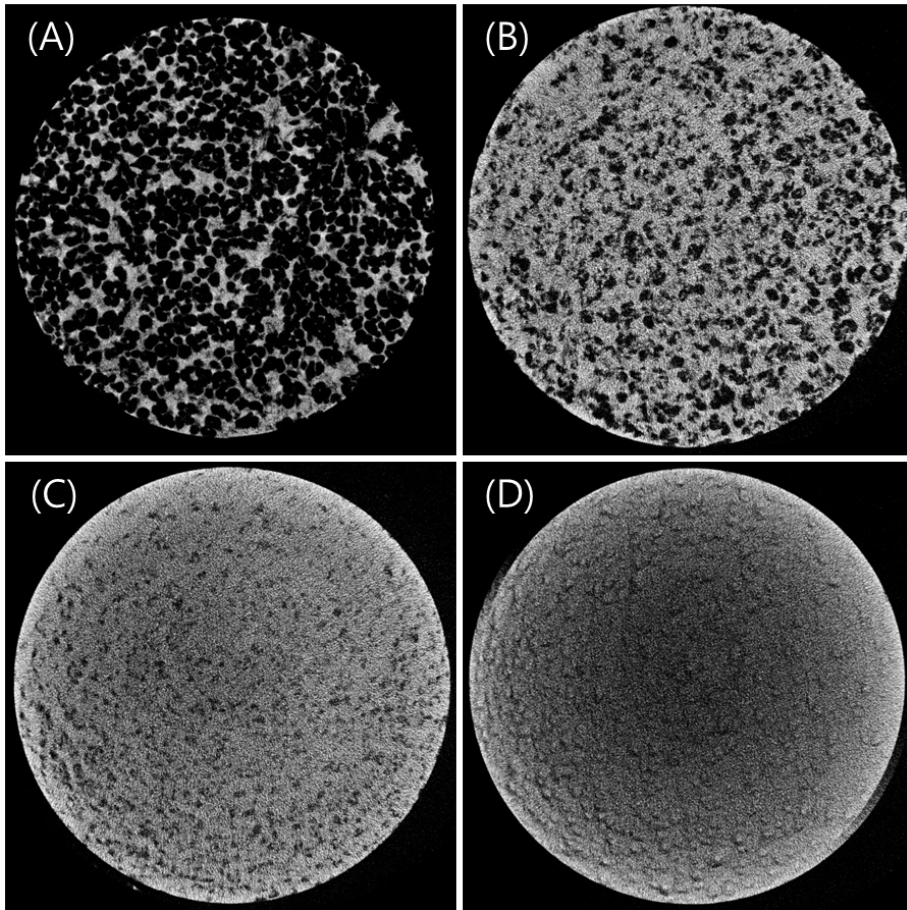


Figure 22. Micro-CT images of the Ti scaffolds with increasing uniaxial pressings; (A) w/o pressing, (B) 500 MPa, (C) 1000 MPa and (D) 2000 MPa.

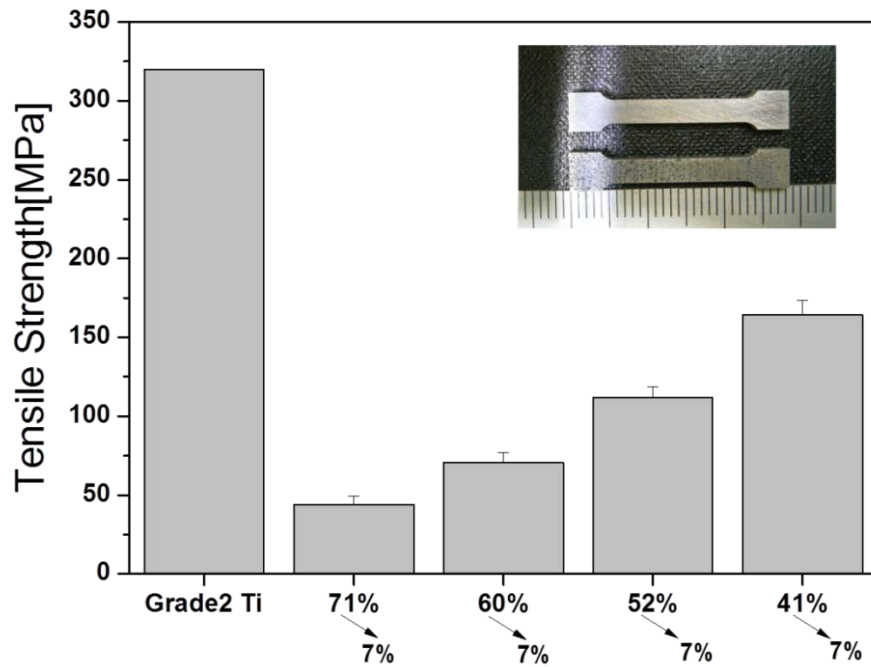


Figure 23. Tensile strength of the dense Ti scaffolds as a function of the initial porosity.

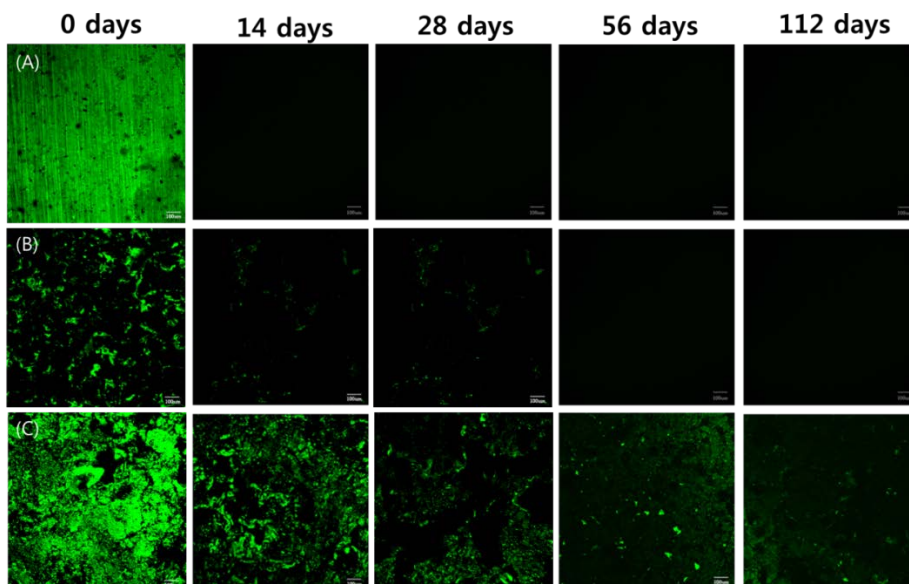


Figure 24. Typical CLSM images of GFP loaded Ti scaffolds at 0, 14, 28 56, and 112 days post-loading. (A) GFP-adsorbed as-received Ti, (B) GFP-loaded porous Ti and (C) GFP-embedded densified Ti.

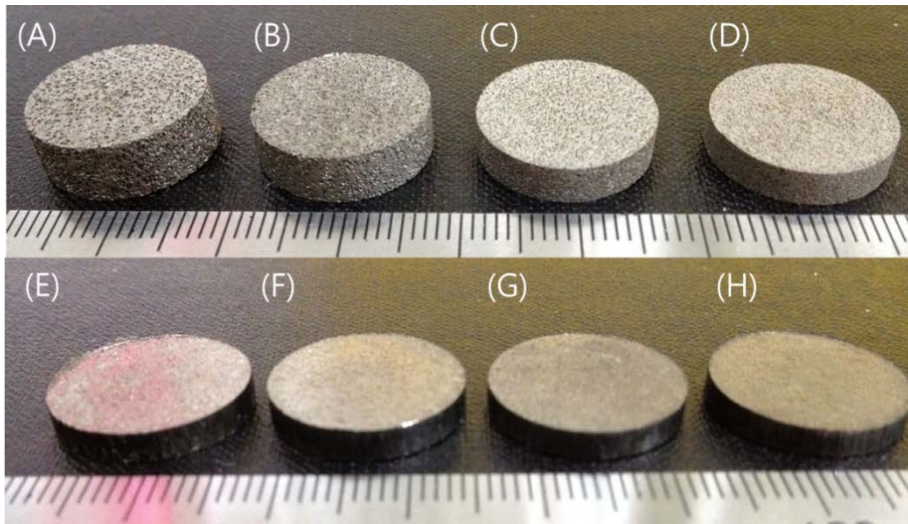


Figure 25. Typical optical image of the porous ((A) P71, (B) P60, (C) P52 and (D) P43) and densified Ti scaffolds ((E) D71, (F) D60, (G) D52 and (H) D43) produced with various initial porosity.

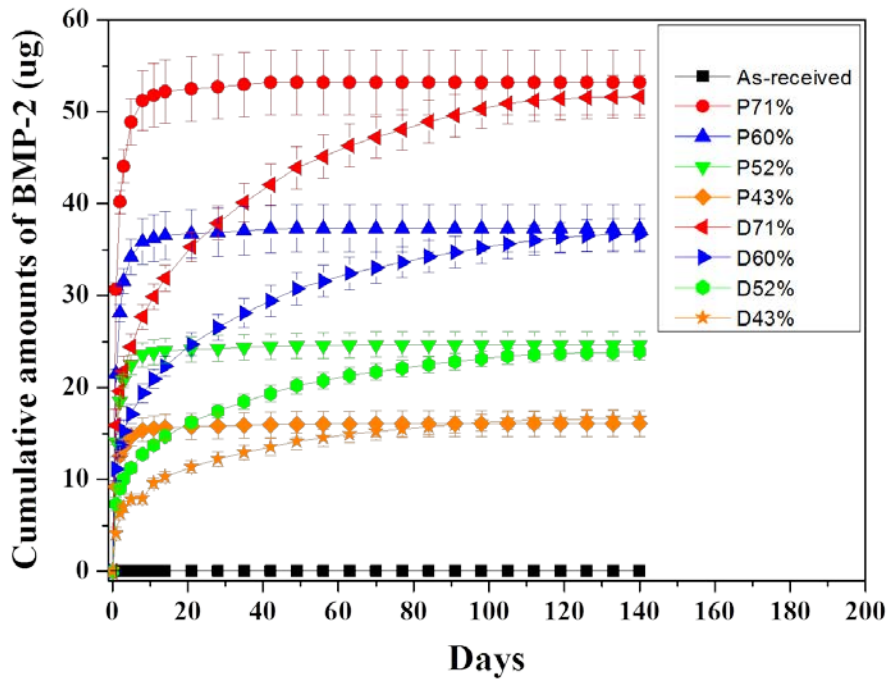


Figure 26. Cumulative amounts of BMP-2 released from as-received, porous and densified Ti as a function of time (n = 5).

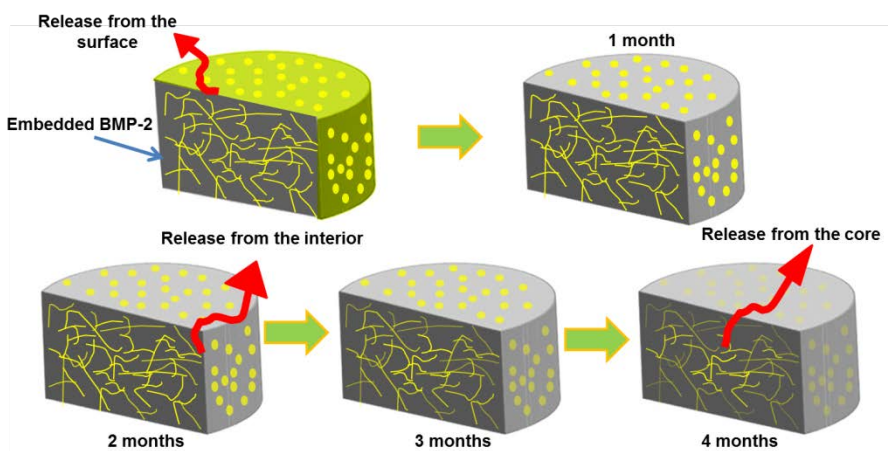


Figure 27. Schematic of sustained growth factor release from densified Ti scaffold.

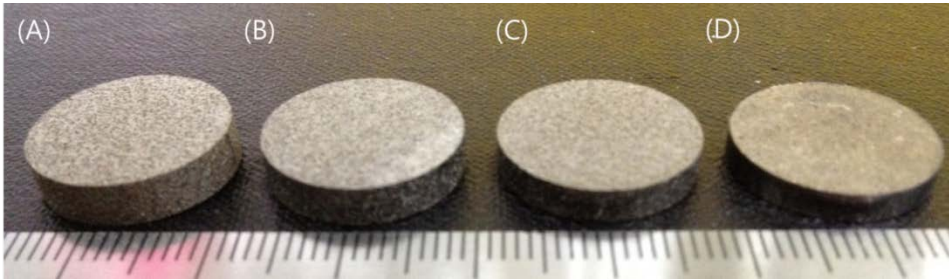


Figure 28. Typical optical images of the 52% porous Ti scaffolds with varying densifications: (A) as is, (B) densified to 42%, (C) 24% and (D) 7%.

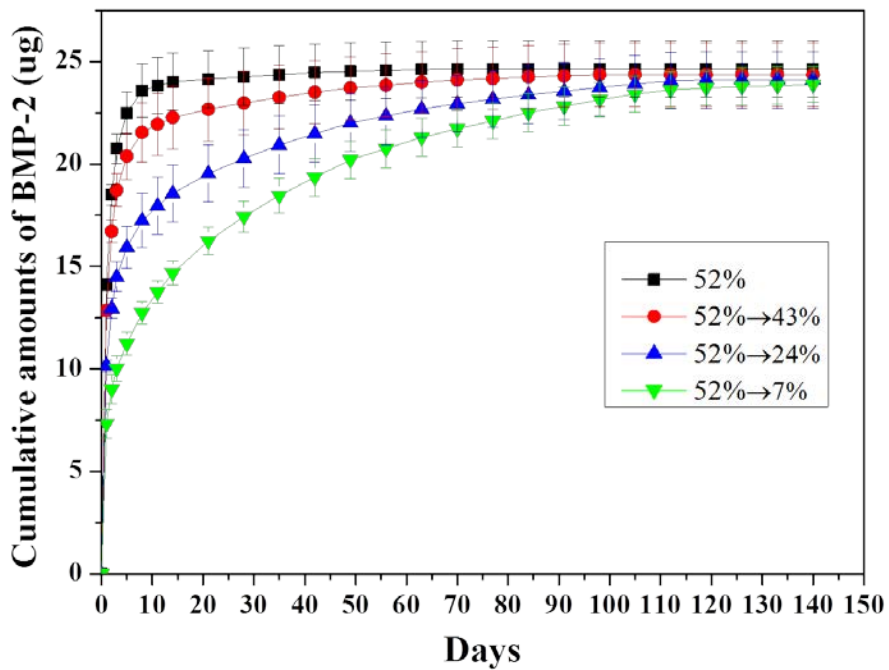


Figure 29. Cumulative amounts of BMP-2 released from densified Ti scaffolds as a function of time (n = 5).

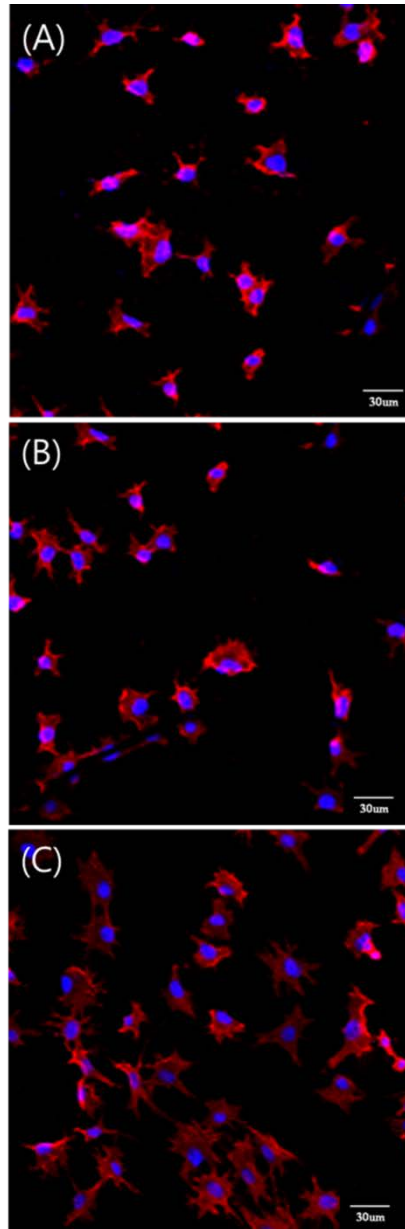


Figure 30. CLSM images of cellular attachment of the (A) as-received Ti, (B) BMP-2-adsorbed as-received Ti and (C) BMP-2-embedded densified Ti after culturing for 3 h.

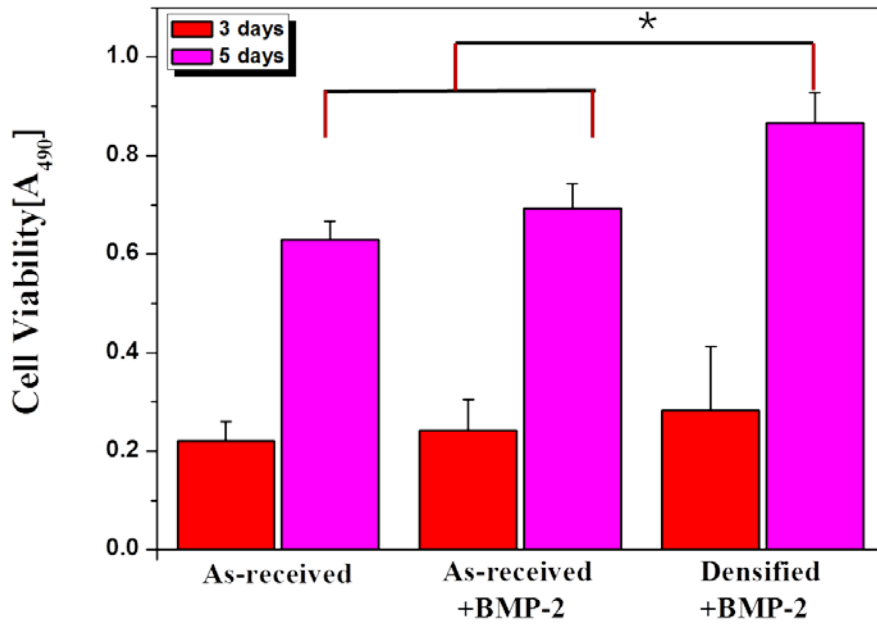


Figure 31. Cell proliferation level of MC3T3-E1 cells of as-received Ti, BMP-2-adsorbed as-received Ti and BMP-2-embedded densified Ti after culturing for 3 and 5 days, *p < 0.05.

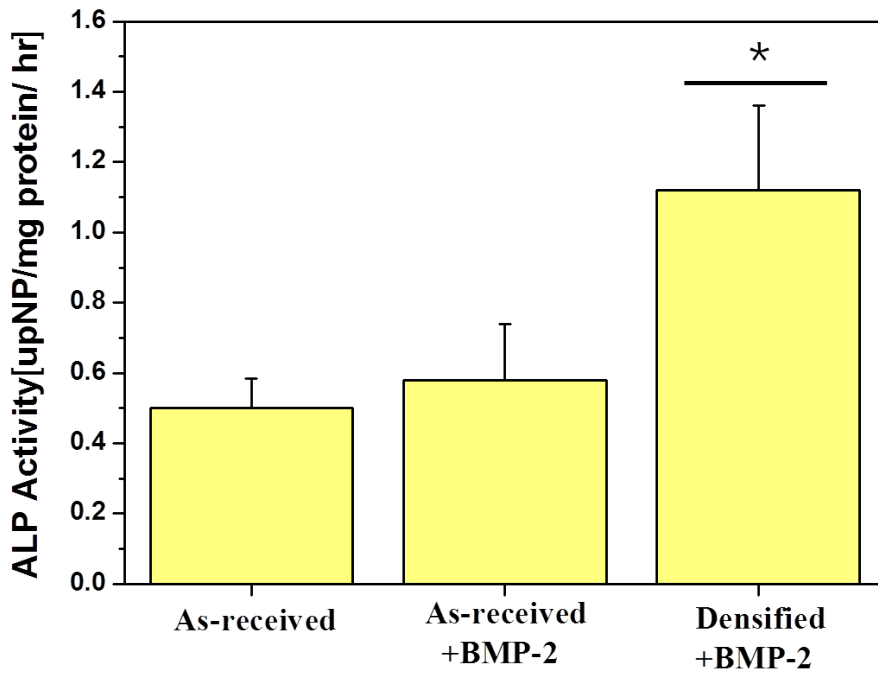


Figure 32. ALP activity of MC3T3-E1 cells of as-received Ti, BMP-2-adsorbed as-received Ti and BMP-2-embedded densified Ti after culturing for 10 days, * $p < 0.05$.

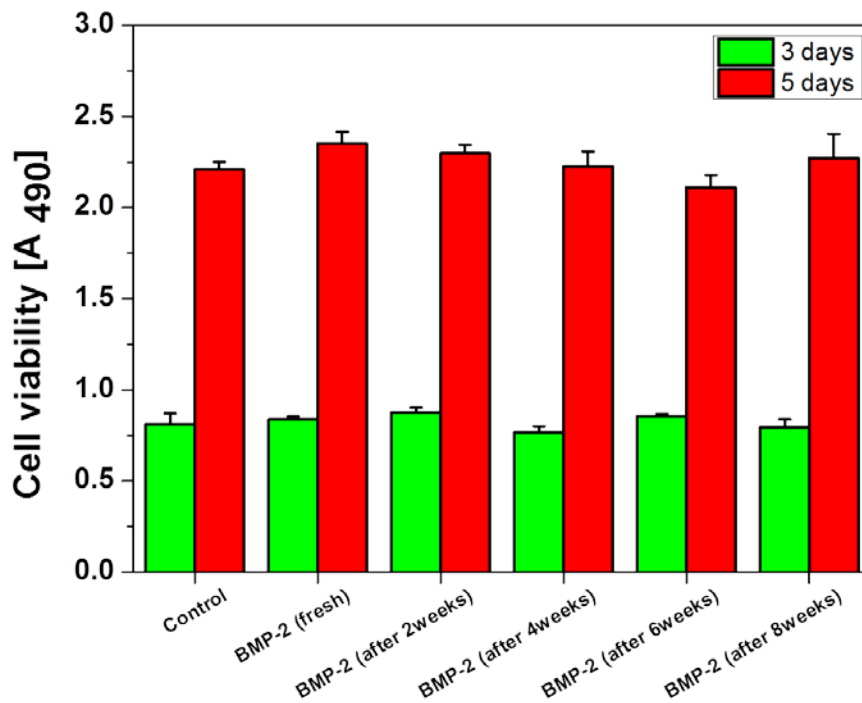


Figure 33. Cell proliferation level of MC3T3-E1 cells of well without BMP-2 (negative control), with BMP-2 (positive control), and with released BMP-2 collected periodically after culturing for 3 and 5 days.

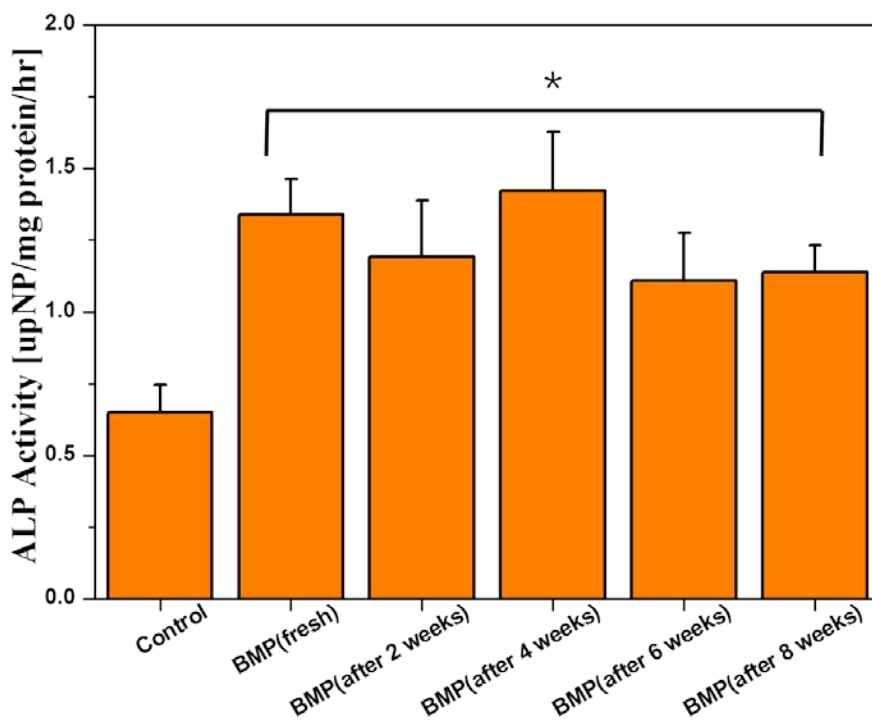


Figure 34. ALP activity of MC3T3-E1 cells of well without BMP-2 (negative control), with BMP-2 (positive control), and with released BMP-2 collected periodically after culturing for 10 days, * $p < 0.05$.

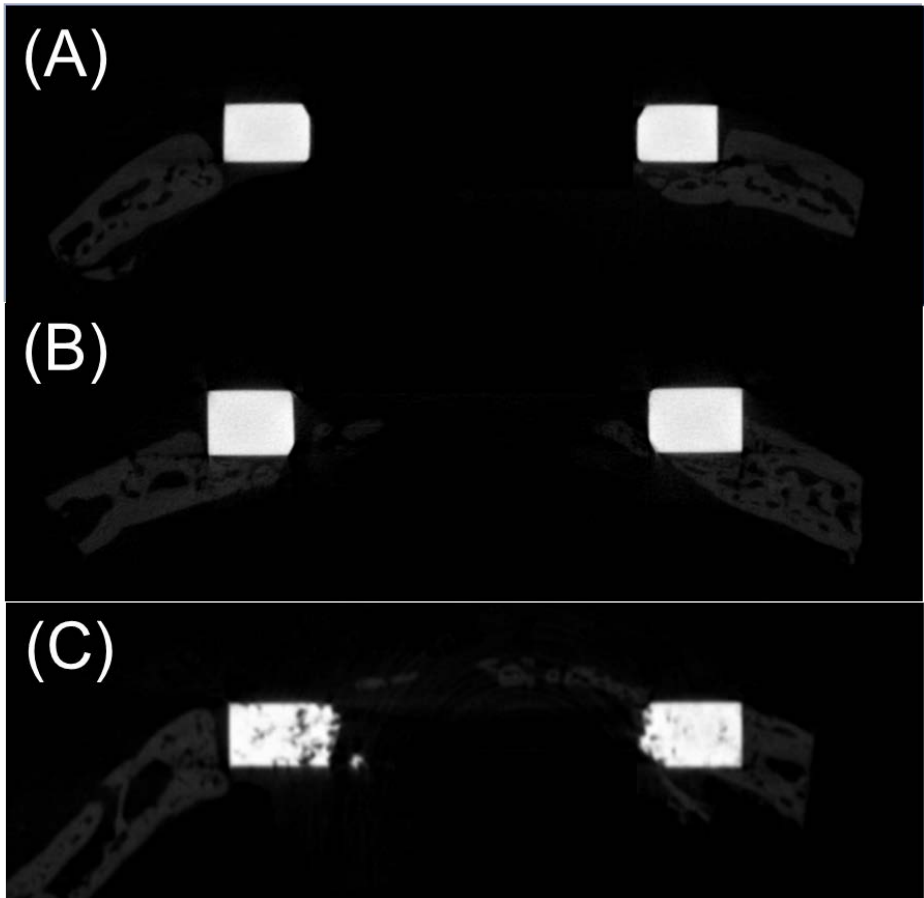


Figure 35. Micro-CT cross-section of a representative rabbit calvaria after 6 weeks of healing (A) as-received Ti (control), (B) BMP-2-adsorbed as-received Ti and (C) BMP-2-embedded densified Ti.

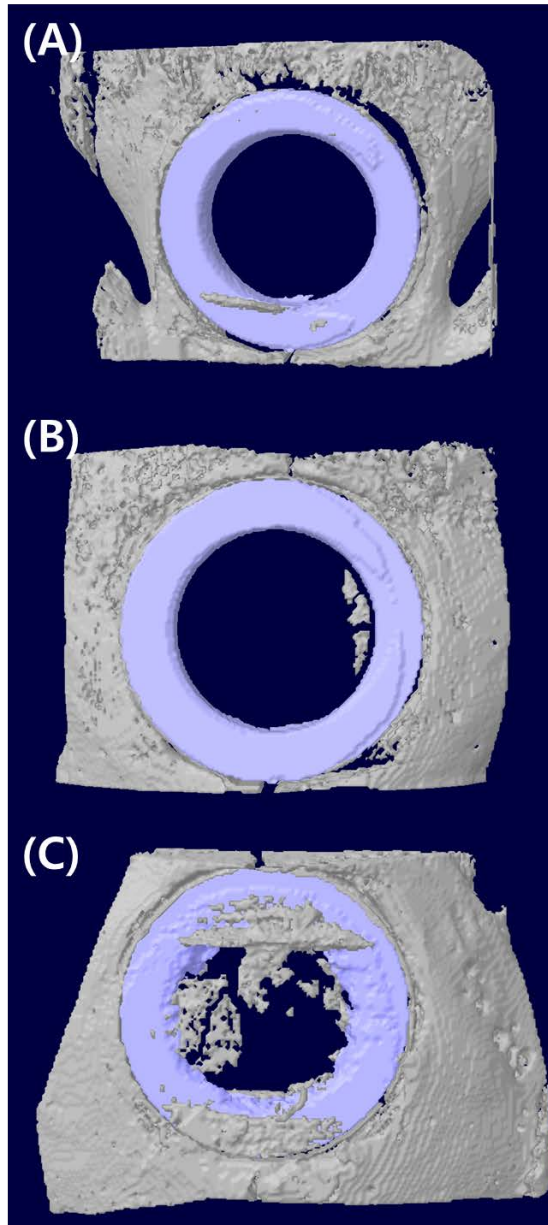


Figure 36. Micro-CT 3-D reconstructions of the rabbit calvaria and implants retrieved at 6 weeks after implantation. (A) as-received Ti (control), (B) BMP-2-adsorbed as-received Ti and (C) BMP-2-embedded densified Ti.

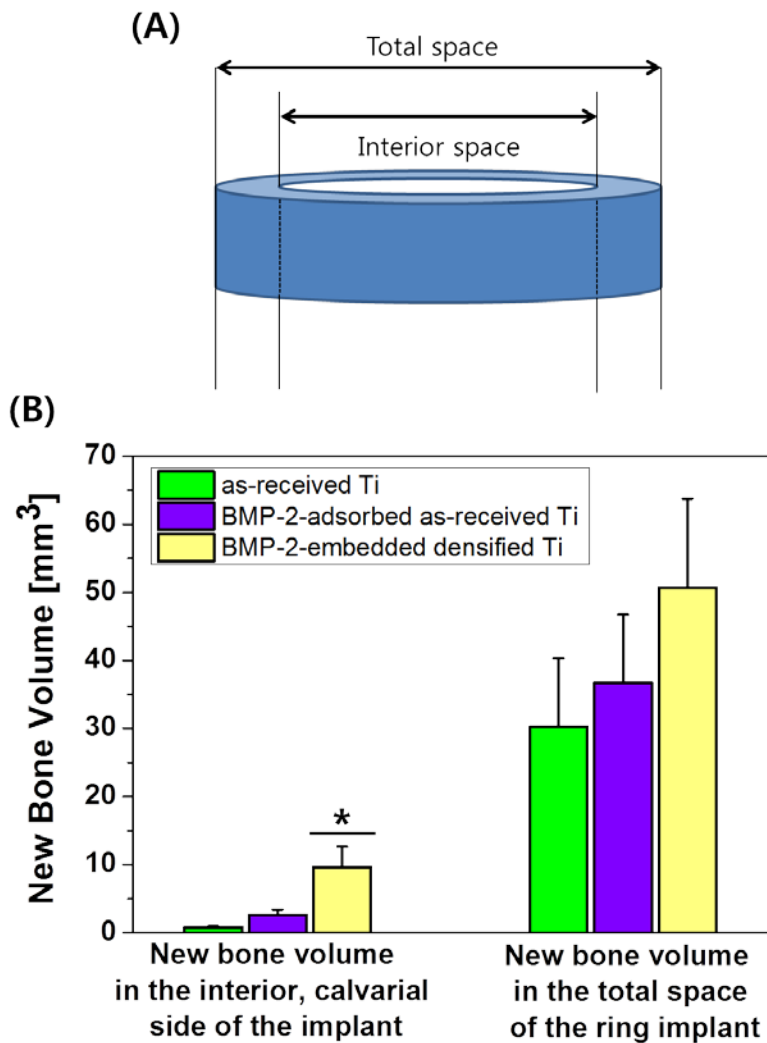


Figure 37. (A) The new bone volume was separately quantified for the interior, calvarial side of the ring implant and the total space of ring implant as shown in the diagram. (B) The average volume of new bone in the interior, calvarial side of the implant and total space of the ring implants for the three different types at 6 weeks determined by micro-CT, * $p < 0.05$.

Chapter 4.

Conclusions

In this study, porous Ti scaffolds with a uniform porous structure were produced by dynamic freeze casting, in which Ti/camphene slurries with a range of initial Ti contents (15, 20, and 25 vol%) were frozen in rotation at 44 °C for 12 h. This method allowed for the extensive growth of camphene crystals and the uniform construction of walls made of Ti particles. All the fabricated samples showed spherical-like pores surrounded by dense Ti walls that were uniformly formed after sintering at 1300 °C for 2 h in a vacuum. The porosity decreased from 71 to 52 vol% with an increase in Ti content from 15 to 25 vol%, whereas the pore size decreased from 362 to 95 μm. On the other hand, the compressive strength and stiffness increased considerably from 57 ± 4 to 183 ± 6 MPa and from 1.3 ± 0.5 to 5.0 ± 0.8 GPa, respectively, due to the decrease in the porosity of the samples.

In the second study, the potential of the Ti scaffolds for the delivery of growth factor such as BMP-2 was examined. Porous Ti scaffold was soaked in a solution containing BMP-2 in a vacuum and was densified to control the release rate of BMP-2. By SEM observation, porosity and pore size of densified Ti decreased with an increase in pressure. The tensile strengths of the densified scaffolds range from 44 to 164 MPa, which are similar to the mechanical properties of the human cortical bone. GFP was used to analyze the growth factor loading capability of the densified Ti samples. Through CLSM imaging, the densified titanium samples showed prolonged release (up to 16 weeks) of the loaded GFP which were slowly released from the internal pores. The release of BMP-2 from the BMP-2-embedded densified Ti was relatively steady in which considerable amounts

of BMP-2 were released even after 20 weeks. The *in vitro* cellular responses of the MC3T3-E1 pre-osteoblasts were examined using a cell attachment, a cell proliferation assay and an alkaline phosphatase (ALP) assay, and these results demonstrated that the BMP-2-embedded densified Ti also enhanced cell adhesion, proliferation and differentiation levels. Additional *in vitro* cell tests were performed to verify that BMP-2 is maintaining its biological functions even after 8 weeks of release. . To examine the potential of BMP-2-embedded densified Ti as a growth factor carrier, the *in vivo* animal test was conducted using rabbit calvarial defect model. According to micro-CT images, BMP-2-embedded densified Ti ring implant showed better integration with the calvaria on the surface compared to the as-received Ti implant. Moreover, better cell ingrowth was observed on the densified sample compared to that of the control sample. 3-D analysis showed that the new bone volume of the densified samples was approximately 1.5 times greater than that of the as-received control sample.

This study demonstrates that freeze casting is quite useful for producing porous Ti scaffolds with a various pore structure and those scaffolds have potentials as bone scaffold materials. BMP-2-embedded densified Ti could be used as a potential bone scaffold with growth factor delivery system in the dental and orthopedic field.

References

- [1] Chen D, Zhao M, Mundy GR. Bone morphogenetic proteins. *Growth factors* 2004;22:233-41.
- [2] Mayer L, Wehner E. An experimental study of osteogenesis. *The Journal of Bone & Joint Surgery* 1914;2:213-44.
- [3] Friedlaender G. Bone grafts. The basic science rationale for clinical applications. *The Journal of bone and joint surgery American volume* 1987;69:786.
- [4] Finkemeier CG. Bone-grafting and bone-graft substitutes. *The Journal of Bone & Joint Surgery* 2002;84:454-64.
- [5] Stevenson S. Biology of bone grafts. *The Orthopedic clinics of North America* 1999;30:543.
- [6] Brown KL, Cruess RL. Bone and cartilage transplantation in orthopaedic surgery. A review. *The Journal of bone and joint surgery* 1982;64:270.
- [7] Damien CJ, Parsons JR. Bone graft and bone graft substitutes: a review of current technology and applications. *Journal of Applied Biomaterials* 1991;2:187-208.
- [8] Lane JM, Tomin E, Bostrom MPG. Biosynthetic bone grafting. *Clinical orthopaedics and related research* 1999;367:S107.
- [9] Arrington ED, Smith WJ, Chambers HG, Bucknell AL, Davino NA. Complications of iliac crest bone graft harvesting. *Clinical orthopaedics and related research* 1996;329:300.

- [10] Mendicino RW, Leonheart E, Shromoff P. Techniques for harvesting autogenous bone grafts of the lower extremity. *The Journal of foot and ankle surgery* 1996;35:428-35.
- [11] Brantigan JW, Cunningham BW, Warden K, McAfee PC, Steffee A. Compression strength of donor bone for posterior lumbar interbody fusion. *Spine* 1993;18:1213.
- [12] Lane JM, Sandhu H. Current approaches to experimental bone grafting. *The Orthopedic clinics of North America* 1987;18:213.
- [13] Prolo DJ, Rodrigo JJ. Contemporary bone graft physiology and surgery. *Clinical orthopaedics and related research* 1985;200:322.
- [14] Kalita SJ, Bose S, Hosick HL, Bandyopadhyay A. Development of controlled porosity polymer-ceramic composite scaffolds via fused deposition modeling. *Materials Science and Engineering: C* 2003;23:611-20.
- [15] Zhang R, Ma PX. Poly α -hydroxyl acids/hydroxyapatite porous composites for bone-tissue engineering. I. Preparation and morphology. 1999.
- [16] Frosch KH, Stürmer KM. Metallic biomaterials in skeletal repair. *European Journal of Trauma* 2006;32:149-59.
- [17] Long M, Rack H. Titanium alloys in total joint replacement-a materials science perspective. *BIOMATERIALS-GUILDFORD-* 1998;19:1621-39.
- [18] Niinomi M. Recent metallic materials for biomedical applications. *Metallurgical and materials transactions A* 2002;33:477-86.
- [19] Nouri A, Hodgson PD, Wen C. Biomimetic porous titanium scaffolds for orthopaedic and dental applications: In-Tech; 2010.

- [20] Niinomi M, Fukunaga KI, Tono G, Koike J, Eylon D, Fujishiro S. Effect of microstructure on fracture characteristics of Ti-6Al-2Sn-2Zr-2Mo-2Cr-Si. *Metallurgical and materials transactions A* 2001;32:2795-804.
- [21] Centrella M, McCarthy TL, Canalis E. Effects of transforming growth factors on bone cells. *Connective tissue research* 1989;20:267-75.
- [22] Özkaynak E, Schnegelsberg PNJ, Oppermann H. Murine osteogenic protein (OP-1): high levels of mRNA in kidney. *Biochemical and biophysical research communications* 1991;179:116-23.
- [23] Obradovic Wagner D, Sieber C, Bhushan R, Borgermann JH, Graf D, Knaus P. BMPs: from bone to body morphogenetic proteins. *Science Signalling* 2010;3:mr1.
- [24] Zhu G, Guo B, Pan D, Mu Y, Feng S. Expression of bone morphogenetic proteins and receptors in porcine cumulus–oocyte complexes during in vitro maturation. *Animal reproduction science* 2008;104:275-83.
- [25] von Bubnoff A, Cho K. Intracellular BMP signaling regulation in vertebrates: pathway or network? *Developmental biology* 2001;239:1.
- [26] Zhang H, Bradley A. Mice deficient for BMP2 are nonviable and have defects in amnion/chorion and cardiac development. *Development* 1996;122:2977-86.
- [27] Winnier G, Blessing M, Labosky PA, Hogan B. Bone morphogenetic protein-4 is required for mesoderm formation and patterning in the mouse. *Genes & development* 1995;9:2105-16.
- [28] Bandyopadhyay A, Tsuji K, Cox K, Harfe BD, Rosen V, Tabin CJ. Genetic analysis of the roles of BMP2, BMP4, and BMP7 in limb patterning and skeletogenesis. *PLoS genetics* 2006;2:e216.

- [29] Kim RY, Robertson EJ, Solloway MJ. Bmp6 and Bmp7 are required for cushion formation and septation in the developing mouse heart. *Developmental biology* 2001;235:449-66.
- [30] Cao X, Chen D. The BMP signaling and in vivo bone formation. *Gene* 2005;357:1.
- [31] Lu L, Yaszemski MJ, Mikos AG. TGF- β 1 release from biodegradable polymer microparticles: its effects on marrow stromal osteoblast function. *The Journal of Bone and Joint Surgery (American)* 2001;83:S82-S92.
- [32] Elima K. Osteoinductive proteins. *Annals of medicine* 1993;25:395-402.
- [33] Boden SD, Kang J, Sandhu H, Heller JG. Use of recombinant human bone morphogenetic protein-2 to achieve posterolateral lumbar spine fusion in humans: A prospective, randomized clinical pilot trial 2002 Volvo Award in clinical studies. *Spine* 2002;27:2662.
- [34] Bessho K, Carnes D, Cavin R, Ong J. Experimental studies on bone induction using low-molecular-weight poly (DL-lactide-co-glycolide) as a carrier for recombinant human bone morphogenetic protein-2. *Journal of biomedical materials research* 2002;61:61-5.
- [35] Mori M, Isobe M, Yamazaki Y, Ishihara K, Nakabayashi N. Restoration of segmental bone defects in rabbit radius by biodegradable capsules containing recombinant human bone morphogenetic protein-2. *Journal of biomedical materials research* 2000;50:191-8.
- [36] Burdick JA, Mason MN, Hinman AD, Thorne K, Anseth KS. Delivery of osteoinductive growth factors from degradable PEG hydrogels influences osteoblast differentiation and mineralization. *Journal of Controlled Release* 2002;83:53-63.

- [37] Woo BH, Fink BF, Page R, Schrier JA, Jo YW, Jiang G, et al. Enhancement of bone growth by sustained delivery of recombinant human bone morphogenetic protein-2 in a polymeric matrix. *Pharmaceutical research* 2001;18:1747-53.
- [38] Jansen J, Vehof J, Ruhe P, Kroeze-Deutman H, Kuboki Y, Takita H, et al. Growth factor-loaded scaffolds for bone engineering. *Journal of Controlled Release* 2005;101:127-36.
- [39] Yang G, He F, Hu J, Wang X, Zhao S. Effects of biomimetically and electrochemically deposited nano-hydroxyapatite coatings on osseointegration of porous titanium implants. *Oral Surgery, Oral Medicine, Oral Pathology, Oral Radiology, and Endodontology* 2009;107:782-9.
- [40] Lee J, Decker JF, Polimeni G, Cortella CA, Rohrer MD, Wozney JM, et al. Evaluation of implants coated with rhBMP-2 using two different coating strategies: a critical-size supraalveolar peri-implant defect study in dogs. *Journal of clinical periodontology* 2010;37:582-90.
- [41] So K, Takemoto M, Fujibayashi S, Neo M, Kokubo T, Nakamura T. Reinforcement of tendon attachment to bioactive porous titanium by BMP-2-induced ectopic bone formation. *Journal of Biomedical Materials Research Part A* 2009;93:1410-6.
- [42] Li JP, Li SH, De Groot K, Layrolle P. Preparation and characterization of porous titanium. *Key Engineering Materials* 2001;218:51-4.
- [43] Bram M, Stiller C, Buchkremer HP, Stöver D, Baur H. High-Porosity Titanium, Stainless Steel, and Superalloy Parts. *Advanced Engineering Materials* 2000;2:196-9.
- [44] Melican MC, Zimmerman MC, Dhillon MS, Ponnambalam AR,

Curodeau A, Parsons JR. Three-dimensional printing and porous metallic surfaces: A new orthopedic application. *Journal of biomedical materials research* 2001;55:194-202.

[45] Curodeau A, Sachs E, Caldarise S. Design and fabrication of cast orthopedic implants with freeform surface textures from 3-D printed ceramic shell. *Journal of biomedical materials research* 2000;53:525-35.

[46] Pilliar RM. P/M processing of surgical sintered porous surfaces for tissue-to-implant fixation. *International journal of powder metallurgy* 1998;34:33-45.

[47] Liao J, Zhang B. *Porous materials of powder metallurgy*. China: Metallurgy Industry Press 1978.

[48] Galante J, Rostoker W, Lueck R, RAY RD. Sintered fiber metal composites as a basis for attachment of implants to bone. *The Journal of Bone and Joint Surgery (American)* 1971;53:101-14.

[49] Hahn H, Palich W. Preliminary evaluation of porous metal surfaced titanium for orthopedic implants. *Journal of biomedical materials research* 1970;4:571-7.

[50] Yang Y, Tian J, Tian J, Chen Z, Deng X, Zhang D. Preparation of graded porous titanium coatings on titanium implant materials by plasma spraying. *Journal of biomedical materials research* 2000;52:333-7.

[51] Fujibayashi S, Neo M, Kim HM, Kokubo T, Nakamura T. Osteoinduction of porous bioactive titanium metal. *Biomaterials* 2004;25:443-50.

[52] Thieme M, Wieters KP, Bergner F, Scharnweber D, Worch H, Ndop J, et al. Titanium powder sintering for preparation of a porous functionally

graded material destined for orthopaedic implants. *Journal of Materials Science: Materials in Medicine* 2001;12:225-31.

[53] Zhang QY, Liu X, Chen J, Zhang X. Fabrication of porous titanium and biomimetic deposition of calcium phosphate. *Key Engineering Materials* 2002;240:89-92.

[54] Dunand D, Teisen J. *Superplastic foaming of titanium and Ti-6Al-4V*. Cambridge Univ Press; 1998.

[55] Davis N, Teisen J, Schuh C, Dunand D. Solid-state foaming of titanium by superplastic expansion of argon-filled pores. *JOURNAL OF MATERIALS RESEARCH-PITTSBURGH-* 2001;16:1508-19.

[56] Pilliar R, Deporter D, Watson P, Todescan R. The Endopore implant-enhanced osseointegration with a sintered porous-surfaced design. *Oral health* 1998;88:61.

[57] Pilliar RM. Porous-surfaced metallic implants for orthopedic applications. *Journal of biomedical materials research* 1987;21:1.

[58] Nishihara H, Mukai SR, Yamashita D, Tamon H. Ordered macroporous silica by ice templating. *Chemistry of materials* 2005;17:683-9.

[59] Kim JW, Taki K, Nagamine S, Ohshima M. Preparation of poly (L-lactic acid) honeycomb monolith structure by unidirectional freezing and freeze-drying. *Chemical Engineering Science* 2008;63:3858-63.

[60] Ma PX, Zhang R. Microtubular architecture of biodegradable polymer scaffolds. *Journal of biomedical materials research* 2001;56:469-77.

[61] Zhang H, Hussain I, Brust M, Butler MF, Rannard SP, Cooper AI. Aligned two-and three-dimensional structures by directional freezing of

polymers and nanoparticles. *Nature materials* 2005;4:787-93.

[62] Araki K, Halloran JW. New Freeze-Casting Technique for Ceramics with Sublimable Vehicles. *Journal of the American Ceramic Society* 2004;87:1859-63.

[63] Chen R, Wang CA, Huang Y, Ma L, Lin W. Ceramics with Special Porous Structures Fabricated by Freeze-Gelcasting: Using tert-Butyl Alcohol as a Template. *Journal of the American Ceramic Society* 2007;90:3478-84.

[64] Deville S, Saiz E, Nalla RK, Tomsia AP. Freezing as a path to build complex composites. *Science* 2006;311:515-8.

[65] Araki K, Halloran JW. Porous ceramic bodies with interconnected pore channels by a novel freeze casting technique. *Journal of the American Ceramic Society* 2005;88:1108-14.

[66] Song JH, Koh YH, Kim HE, Li LH, Bahn HJ. Fabrication of a Porous Bioactive Glass–Ceramic Using Room-Temperature Freeze Casting. *Journal of the American Ceramic Society* 2006;89:2649-53.

[67] Koh YH, Song JH, Lee EJ, Kim HE. Freezing Dilute Ceramic/Camphene Slurry for Ultra-High Porosity Ceramics with Completely Interconnected Pore Networks. *Journal of the American Ceramic Society* 2006;89:3089-93.

[68] Li JC, Dunand DC. Mechanical properties of directionally freeze-cast titanium foams. *Acta Materialia* 2011;59:146-58.

[69] Deville S, Saiz E, Tomsia AP. Ice-templated porous alumina structures. *Acta Materialia* 2007;55:1965-74.

[70] Yook SW, Yoon BH, Kim HE, Koh YH, Kim YS. Porous titanium (Ti)

scaffolds by freezing TiH₂/camphene slurries. *Materials Letters* 2008;62:4506-8.

[71] Yook SW, Kim HE, Koh YH. Fabrication of porous titanium scaffolds with high compressive strength using camphene-based freeze casting. *Materials Letters* 2009;63:1502-4.

[72] Jung HD, Yook SW, Kim HE, Koh YH. Fabrication of titanium scaffolds with porosity and pore size gradients by sequential freeze casting. *Materials Letters* 2009;63:1545-7.

[73] Fu Q, Rahaman MN, Dogan F, Bal BS. Freeze casting of porous hydroxyapatite scaffolds. I. Processing and general microstructure. *Journal of Biomedical Materials Research Part B: Applied Biomaterials* 2007;86:125-35.

[74] Koch D, Andresen L, Schmedders T, Grathwohl G. Evolution of porosity by freeze casting and sintering of sol-gel derived ceramics. *Journal of sol-gel science and technology* 2003;26:149-52.

[75] Deville S. Freeze-Casting of Porous Ceramics: A Review of Current Achievements and Issues. *Advanced Engineering Materials* 2008;10:155-69.

[76] Liu X, Chu PK, Ding C. Surface modification of titanium, titanium alloys, and related materials for biomedical applications. *Materials Science and Engineering: R: Reports* 2004;47:49-121.

[77] Ryan G, Pandit A, Apatsidis DP. Fabrication methods of porous metals for use in orthopaedic applications. *Biomaterials* 2006;27:2651-70.

[78] Chen Y, Feng B, Zhu Y, Weng J, Wang J, Lu X. Fabrication of porous titanium implants with biomechanical compatibility. *Materials Letters* 2009;63:2659-61.

[79] Lee JH, Kim HE, Shin KH, Koh YH. Improving the strength and biocompatibility of porous titanium scaffolds by creating elongated pores coated with a bioactive, nanoporous TiO₂ layer. *Materials Letters* 2010;64:2526-9.

[80] Fukuda A, Takemoto M, Saito T, Fujibayashi S, Neo M, Pattanayak DK, et al. Osteoinduction of porous Ti implants with channel structure fabricated by selective laser melting. *Acta Biomaterialia* 2011.

[81] Ryan GE, Pandit AS, Apatsidis DP. Porous titanium scaffolds fabricated using a rapid prototyping and powder metallurgy technique. *Biomaterials* 2008;29:3625-35.

[82] Xiong J, Li Y, Wang X, Hodgson P, Wen C. Mechanical properties and bioactive surface modification via alkali-heat treatment of a porous Ti-18Nb-4Sn alloy for biomedical applications. *Acta Biomaterialia* 2008;4:1963-8.

[83] Yoon BH, Choi WY, Kim HE, Kim JH, Koh YH. Aligned porous alumina ceramics with high compressive strengths for bone tissue engineering. *Scripta Materialia* 2008;58:537-40.

[84] Imwinkelried T. Mechanical properties of open-pore titanium foam. *Journal of Biomedical Materials Research Part A* 2007;81:964-70.

[85] Yasko AW, Lane J, Fellingner E, Rosen V, Wozney J, Wang E. The healing of segmental bone defects, induced by recombinant human bone morphogenetic protein (rhBMP-2). A radiographic, histological, and biomechanical study in rats. *The Journal of bone and joint surgery American volume* 1992;74:659.

[86] Schimandle JH, Boden SD, Hutton WC. Experimental spinal fusion

with recombinant human BMP-2. *Spine* 1995;20:1326.

[87] Israel DI, Nove J, Kerns KM, Moutsatsos IK, Kaufman RJ. Expression and characterization of bone morphogenetic protein-2 in Chinese hamster ovary cells. *Growth Factors* 1992;7:139-50.

[88] Bessho K, Konishi Y, Kaihara S, Fujimura K, Okubo Y, Iizuka T. Bone induction by *Escherichia coli*-derived recombinant human bone morphogenetic protein-2 compared with Chinese hamster ovary cell-derived recombinant human bone morphogenetic protein-2. *British Journal of Oral and Maxillofacial Surgery* 2000;38:645-9.

[89] Puleo DA. Dependence of mesenchymal cell responses on duration of exposure to bone morphogenetic protein-2 in vitro. *Journal of cellular physiology* 1997;173:93-101.

[90] Wang EA, Rosen V, D'Alessandro JS, Bauduy M, Cordes P, Harada T, et al. Recombinant human bone morphogenetic protein induces bone formation. *Proceedings of the National Academy of Sciences* 1990;87:2220.

[91] Cook SD, Baffes GC, Wolfe MW, SAMPATH TK, Rueger DC. Recombinant human bone morphogenetic protein-7 induces healing in a canine long-bone segmental defect model. *Clinical orthopaedics and related research* 1994;301:302.

[92] Winn SR, Uludag H, Hollinger JO. Carrier systems for bone morphogenetic proteins. *Clinical orthopaedics and related research* 1999;367:S95.

[93] Seeherman H, Wozney J, Li R. Bone morphogenetic protein delivery systems. *Spine* 2002;27:S16.

[94] Lindholm T, Gao T. Functional carriers for bone morphogenetic

proteins. Helsinki: Finnish Surgical Society, 1976-; 1993. p. 3-12.

[95] Winn SR, Uludag H, Hollinger JO. Sustained release emphasizing recombinant human bone morphogenetic protein-2. *Advanced drug delivery reviews* 1998;31:303-18.

[96] Fujimura K, Bessho K, Kusumoto K, Ogawa Y, Iizuka T. Experimental studies on bone inducing activity of composites of atelopeptide type I collagen as a carrier for ectopic osteoinduction by rhBMP-2. *Biochemical and biophysical research communications* 1995;208:316-22.

[97] Zhang R, Xu D, Landeryou T, Toth C, Dimaano N, Berry J, et al. Ectopic bone formation using osteogenic protein-1 carried by a solution precipitated hydroxyapatite. *Journal of Biomedical Materials Research Part A* 2004;71:412-8.

[98] Simon Z, Deporter DA, Pilliar RM, Clokie CM. Heterotopic bone formation around sintered porous-surfaced Ti-6Al-4V implants coated with native bone morphogenetic proteins. *Implant Dentistry* 2006;15:265.

[99] Liu Y, De Groot K, Hunziker E. BMP-2 liberated from biomimetic implant coatings induces and sustains direct ossification in an ectopic rat model. *Bone* 2005;36:745-57.

[100] Buser D, Schenk R, Steinemann S, Fiorellini J, Fox C, Stich H. Influence of surface characteristics on bone integration of titanium implants. A histomorphometric study in miniature pigs. *Journal of biomedical materials research* 1991;25:889-902.

[101] Meffert R. Do implant surfaces make a difference? *Current opinion in periodontology* 1997;4:104.

[102] Oonishi H, Yamamoto M, Ishimaru H, Tsuji E, Kushitani S, Aono M,

et al. The effect of hydroxyapatite coating on bone growth into porous titanium alloy implants. *Journal of Bone & Joint Surgery, British Volume* 1989;71:213-6.

[103] Cochran D, Schenk R, Lussi A, Higginbottom F, Buser D. Bone response to unloaded and loaded titanium implants with a sandblasted and acid-etched surface: a histometric study in the canine mandible. *Journal of biomedical materials research* 1998;40:1-11.

[104] Klein C, Patka P, Wolke J, de Blicq-Hogervorst J, De Groot K. Long-term in vivo study of plasma-sprayed coatings on titanium alloys of tetracalcium phosphate, hydroxyapatite and α -tricalcium phosphate. *Biomaterials* 1994;15:146-50.

[105] Coombes A, Meikle M. Resorbable synthetic polymers s replacements for bone graft. *Clinical materials* 1994;17:35-67.

[106] Burg KJL, Porter S, Kellam JF. Biomaterial developments for bone tissue engineering. *Biomaterials* 2000;21:2347-59.

[107] Takahashi Y, Yamamoto M, Tabata Y. Enhanced osteoinduction by controlled release of bone morphogenetic protein-2 from biodegradable sponge composed of gelatin and β -tricalcium phosphate. *Biomaterials* 2005;26:4856-65.

[108] Armstrong L, Hughes O, Yung S, Hyslop L, Stewart R, Wappler I, et al. The role of PI3K/AKT, MAPK/ERK and NF κ B signalling in the maintenance of human embryonic stem cell pluripotency and viability highlighted by transcriptional profiling and functional analysis. *Human molecular genetics* 2006;15:1894-913.

[109] Vandermoere F, El Yazidi-Belkoura I, Slomianny C, Demont Y,

Bidaux G, Adriaenssens E, et al. The valosin-containing protein (VCP) is a target of Akt signaling required for cell survival. *Journal of Biological Chemistry* 2006;281:14307-13.

[110] Vandermoere F, El Yazidi-Belkoura I, Demont Y, Slomianny C, Antol J, Lemoine J, et al. Proteomics exploration reveals that actin is a signaling target of the kinase Akt. *Molecular & Cellular Proteomics* 2007;6:114-24.

[111] Yang XB, Whitaker MJ, Sebald W, Clarke N, Howdle SM, Shakesheff KM, et al. Human osteoprogenitor bone formation using encapsulated bone morphogenetic protein 2 in porous polymer scaffolds. *Tissue Engineering* 2004;10:1037-45.

[112] Park YJ, Kim KH, Lee JY, Ku Y, Lee SJ, Min BM, et al. Immobilization of bone morphogenetic protein-2 on a nanofibrous chitosan membrane for enhanced guided bone regeneration. *Biotechnology and applied biochemistry* 2006;43:17-24.

[113] Jones AA, Buser D, Schenk R, Wozney J, Cochran DL. The effect of rhBMP-2 around endosseous implants with and without membranes in the canine model. *Journal of periodontology* 2006;77:1184-93.

[114] Zhang C, Hu YY, Cui FZ, Zhang SM, Ruan DK. A study on a tissue-engineered bone using rhBMP-2 induced periosteal cells with a porous nano-hydroxyapatite/collagen/poly (L-lactic acid) scaffold. *Biomedical Materials* 2006;1:56.

[115] Kawai T, Miki A, Ohno Y, Umemura M, Kataoka H, Kurita S, et al. Osteoinductive activity of composites of bone morphogenetic protein and pure titanium. *Clinical orthopaedics and related research* 1993;290:296.

[116] Becker J, Kirsch A, Schwarz F, Chatzinikolaidou M, Rothamel D,

Lekovic V, et al. Bone apposition to titanium implants biocoated with recombinant human bone morphogenetic protein-2 (rhBMP-2). A pilot study in dogs. *Clinical oral investigations* 2006;10:217-24.

[117] Sachse A, Wagner A, Keller M, Wagner O, Wetzel WD, Layher F, et al. Osteointegration of hydroxyapatite-titanium implants coated with nonglycosylated recombinant human bone morphogenetic protein-2 (BMP-2) in aged sheep. *Bone* 2005;37:699-710.

[118] Lan J, Wang Z, Shi B, Xia H, Cheng X. The influence of recombinant human BMP-2 on bone-implant osseointegration: biomechanical testing and histomorphometric analysis. *International journal of oral and maxillofacial surgery* 2007;36:345-9.

[119] Morra M, Cassinelli C, Meda L, Fini M, Giavaresi G, Giardino R. Surface analysis and effects on interfacial bone microhardness of collagen-coated titanium implants: a rabbit model. *The International journal of oral & maxillofacial implants* 2005;20:23.

[120] Hanisch O, Sorensen RG, Kinoshita A, Spiekermann H, Wozney JM, Wikesjö UME. Effect of recombinant human BMP-2 in dehiscence defects with non-submerged immediate implants: an experimental study in *Cynomolgus* monkeys. *Journal of periodontology* 2003;74:648-57.

[121] Wikesjö UME, Lim WH, Thomson RC, Cook AD, Wozney JM, Hardwick WR. Periodontal repair in dogs: evaluation of a bioabsorbable space-providing macro-porous membrane with recombinant human bone morphogenetic protein-2. *Journal of periodontology* 2003;74:635-47.

[122] Tessmar J, Kellner K, Schulz MB, Blunk T, Göpferich A. Toward the development of biomimetic polymers by protein immobilization: PEGylation of insulin as a model reaction. *Tissue engineering* 2004;10:441-53.

Curriculum Vitae

Name: Hyun-Do Jung

Date of Birth: August. 22th. 1985

Nationality: Republic of Korea

EDUCATION

Seoul National University, Seoul, Korea

Ph.D. in Materials Science and Engineering, Anticipated February 2013

Advisor: Professor Hyoun-ee Kim

Dissertation: Biomedical Titanium Implants Eluting Growth Factors for Long Period Time

Seoul National University, Seoul, Korea

B.S. in Materials Science and Engineering, February 2008

Dissertation: Silica Xerogel & PCL Bioactive Composites by sol-gel synthesis

RESEARCH INTERESTS

- Fabrication of porous materials
- Metallurgy and ceramic processing
- Inorganic-organic hybrid biomaterials
- Effective delivery of growth factors and the resulting *in vitro* and *in vivo* behaviors

- Biological evaluations of porous materials

TECHNICAL SKILLS

- *Material Processing*

Porous scaffolds: Freeze casting, Replication, Spark plasma sintering, Extrusion

Surface treatment: Spin coating, Electrospinning, Micro arc oxidation, Sol-gel derived silica xerogel

Other: Cold press, Cold isostatic press, furnaces, Hot-press, CNC machine

- *Material Characterization*

Scanning Electron Microscope (SEM), Confocal Laser Scanning Microscope (CLSM), Optical Microscope, X-ray Diffraction (XRD), Micro Computed Tomography (Micro-CT), Fourier Transform-Infrared Spectroscopy (FT-IR), Thermo Gravimetric Analysis (TGA), Differential Scanning Calorimetry (DSC), Mechanical test (Compressive strength, tensile strength, hardness), Goniometer, Microreader, UV spectroscopy

- *Biological Evaluations*

Cellular tests: Cell culture (MC3T3-E1, HUVEC), Cell attachment (Optical, SEM, CLSM), Cell Proliferation Assay (Counting, MTS, MTT), Cell Differentiation Assay (ALP), Drug release assay (ELISA)

Animal test: Anesthesia, Surgery, Suture of rat, guinea pigs and rabbit

Immunohistology: resin block preparation, staining

● *Softwares*

Windows, Microsoft Office, Micro-CT Analysis, Microsoft Office, Origin Lab, SPOT, JCPDS

PUBLICATIONS

1. Kim, S.W., **Jung, H.D.**, Kang, M.H., Estrin Y., Kim, H.E., Koh, Y.H., Fabrication of Porous Ti Implants with Complex Shape, Mater Sci Eng C-Mater 2013 ; 33; 59-63
2. **Jung, H.D.**, Yook, S.W., Jang, T.S., Li, Y., Kim, H.E., Koh, Y.H., Dynamic Freeze Casting for the Production of Porous Titanium(Ti) Scaffolds, Mater Sci Eng C-Mater 2013
3. Pham V. H., Jang, T.S., **Jung, H.D.**, Kim, H.E., Koh, Y.H., Creation of Nanoporous Tantalum (Ta)-incorporated Titanium (Ti) Surface onto Ti Implants by Sputtering of Ta in Ar under Extremely High Negative Substrate Biases, J Mater Chem 2012;22;24798-24804
4. **Jung, H.D.**, Kim, H.E., Koh, Y.H., Production and evaluation of porous titanium scaffolds with 3-dimensional periodic macrochannels coated with microporous TiO₂ layer, Mater Chem Phys 2012;135; 897-902
5. Yook, S.W., **Jung, H.D.**, Kim, H.E., Koh, Y.H., Reverse freeze casting: A new method for fabricating highly porous titanium scaffolds with aligned large pores, Acta Biomater 2012; 8; 2401-2410
6. **Jung, H.D.**, Yook, S.W., Kim, H.E., Koh, Y.H., Fabrication of titanium scaffolds with porosity and pore size gradients by sequential freeze casting, Mater Lett 2009; 63; 1545-1547

KOREA PATENTS

1. Kim, H.E., **Jung, H.D.**, “Method for manufacturing porous metal scaffold using freeze casting, porous metal scaffold manufactured by the same and device for manufacturing porous metal scaffold for living body” 10-2010-0103171
2. Kim, H.E., **Jung, H.D.**, “Implant for drug delivery and the method for manufacturing the same” 10-2010-0103172

PRESENTATIONS

1. **Jung, H.D.**, Yook, S.W., Kim, H.E., Koh, Y.H., Dynamic Freeze Casting of Titanium/Camphene Slurry for Producing Porous Titanium Scaffolds, Oral presentation, International Union of Materials Research Society-International Conference in Asia 2012, 26-31 Aug 2012, Busan, KOREA
2. Kim, S.W., **Jung, H.D.**, Estrin Y., Kim, H.E., Fabrication of Porous Ti Implants with Complex Shape, Oral presentation, International Union of Materials Research Society-International Conference in Asia 2012, 26-31 Aug 2012, Busan, KOREA
3. Kang, M.H., Yook, S.W., **Jung, H.D.**, Estrin Y., Kim, H.E., Fabrication of Porous Magnesium by Spark Plasma Sintering, Oral presentation, International Union of Materials Research Society-International Conference in Asia 2012, 26-31 Aug 2012, Busan, KOREA
4. Kim, S.W., Estrin Y., **Jung, H.D.**, Kim, H.E., Fabrication of Porous Ti Implants with Complex Shape, Oral presentation, 9th World

- Biomaterials Congress, 1-5 Jun 2012, Chengdu, Sichuan, China
5. **Jung, H.D.**, Kim, H.E., Koh, Y.H., Controlled Release of BMP-2 from Dense Titanium, Poster presentation, 9th World Biomaterials Congress, 1-5 Jun 2012, Chengdu, Sichuan, China.
 6. **Jung, H.D.**, Lee, E.J., Kim, H.E., Koh, Y.H., Dense Titanium Implants Embedded with Growth Factors, Poster presentation, Society for Biomaterials 2011 Annual Meeting & Exposition, 13-16 Apr 2011, Orlando, Florida, USA.
 7. **Jung, H.D.**, Kim, H.E., Porous Titanium Scaffolds by Dynamic Freeze Casting for Bone Tissue Engineering, Poster presentation, Society for Biomaterials 2011 Annual Meeting & Exposition, 13-16 Apr 2011, Orlando, Florida, USA.
 8. Kim, S.B., **Jung, H.D.**, Kim, H.E., Koh, Y.H., Porous Titanium Scaffolds With Controlled Pore Size by Combination of Freeze Casting and space Holder Methods, Poster presentation, Society for Biomaterials 2011 Annual Meeting & Exposition, 13-16 Apr 2011, Orlando, Florida, USA.
 9. **Jung, H.D.**, Yook, S.W., Kim, H.E., Koh, Y.H., Biomimetic Structure of Hydroxyapatite Scaffolds by Camphene-based Freeze Casting for Bone Tissue Engineering, Poster presentation, Society for Biomaterials 2010 Annual Meeting and Exposition, 21-24 Apr 2010, Seattle, Washington, USA.

초 록

티타늄은 우수한 기계적 성질, 내부식성 및 생체친화성 때문에 치과 및 정형외과용 금속 임플란트 소재로 활용 가능한 재료이다. 이러한 우수한 성질에도 불구하고 체내 식립 후에 생리적인 환경에 노출되면서 골과의 결합력이 떨어지는 경우가 발생한다. 이러한 문제를 해결하기 위해 성장인자와 같은 생체 분자 재료를 임플란트 표면에 코팅하여 표면의 생체친화성을 증가시켜 골과의 결합력을 높이려는 방법이 연구되고 있다. BMP-2는 이러한 성장인자의 일종으로 세포의 증식과 분화를 촉진하고 특히, 골형성을 유도하는 단백질로서 치과 및 정형외과용 임플란트에 코팅 재료로서 사용될 수 있다. 하지만 임플란트 표면에 코팅된 BMP-2는 쉽게 방출되고 변성되어 그 효과를 제대로 발휘하기 힘들 수 있다. 따라서 본 실험에서는 BMP-2의 장기 방출이 가능한 새로운 형태의 BMP-2 전달체를 제조하였다.

BMP-2의 전달체를 제조하기 위해 우선 균일한 기공 구조와 충분한 연성을 가지는 다공성 티타늄을 동적 동결성형법으로 만들었다. 이 방법에서 다양한 분율(15-25vol%)을 가지는 티타늄/캠핀 슬러리를 44도에서 회전시키며 동결시켜 액상의 캠핀의 고화되었고, 이를 통해 구 형태의 기공이 되는 캠핀이 충분히 균일하게 성장할 수 있었다. 티타늄의 분율이 15 에서 25 vol%으로 증가함에 따라 기공률은 71에서 52%로 줄어들었고 기공 크기는 362 에서 95 μ m로 줄어들었다. 반면 이

때 압축강도는 57에서 183 MPa로, 강성도는 1.3에서 5.0 GPa로 증가하였다. 이러한 실험 결과는 캄핀 기반의 동적 동결성형법을 이용해 제조된 다공성 티타늄이 좋은 정형외과용 임플란트 소재 및 성장 인자 방출용 담지체로 활용될 수 있음을 보여주었다.

나아가 성장인자의 장기간 방출을 가능하게 하기 위해 BMP-2가 담지된 티타늄을 제조하고 평가하였다. 성장인자인 BMP-2의 방출 속도는 티타늄 다공체의 소성 변형 정도를 제어함으로써 조절 되었다. 담지체는 소성 변형이 됨에 따라 기공률과 기공 크기가 줄어들었고 최종적으로는 평균 기공률이 7%, 평균 기공 크기 $12\mu\text{m}$ 였다. 인장강도는 초기 기공률에 따라 달랐고 뼈와 비슷한 강도인 44에서 164 MPa의 범위를 가졌다. 녹색 형광 단백질을 이용하여 성장인자 담지능을 확인하였고 이는 생체유사 용액 내에서의 방출 거동으로 평가되었다. 그 결과 16주 후에도 표면 기공에서 녹색 형광이 확인되었고 이는 담지체로서의 가능성이 충분함을 증명한 것이다. 이를 바탕으로 BMP-2를 담지체에 담지하여 방출 실험을 진행하였다. 소성변형이 안된 경우에는 BMP-2가 2주만에 방출된 반면 소성변형을 한 경우에는 20주까지 방출되는 것을 확인할 수 있었다. 또한 초기 기공률의 차이에 따라 담지량의 제어가 가능했고 소성 변형 정도에 따라 방출 속도를 조절할 수 있었다.

세포 초기 접착, 증식 및 분화능 평가 실험을 통하여 우수한 생체 친화성을 확인할 수 있었다. 방출된 BMP-2의 변성 여부를 세포 증식 및 분화능 평가 실험을 통해 확인을 하였고 8주까지 BMP-2가 변성없이 본연의 생체적 특성을 유지하고 있음을 확인할

수 있었다. 동물실험에서는 토끼의 두개골에 결함을 발생시켜 뼈의 증식을 살펴봄으로써, 이식 6주 후 BMP-2가 담지체에서 우수한 골재생능을 확인하여 볼 수 있었다.

따라서 본 연구를 통해, 동적 동결성형법을 이용해 성장 인자 방출용 담지체로 사용 가능한 다공성 티타늄을 제조할 수 있으며, 다공성 티타늄에 성장 인자를 담지 및 장기간 전달할 수 있으며, 이를 통하여 특성화된 치과 및 정형외과용 임플란트 소재로 사용될 수 있음을 보여주었다.

주요어: 타이타늄, 동결성형법, 다공성 금속, 생체적합성, 방출 거동, 골 형성 유도 인자

학 번: 2008-20686

감사의 글 (Acknowledgement)

기대와 호기심으로 시작했던 대학원 생활에 어느덧 종지부를 찍을 시간이 다가왔습니다. 어느덧 5년이라는 시간이 흐르고 많은 분들의 도움으로 학위 과정을 무사히 마치고 이제서야 잠시 뒤를 돌아볼 수 있는 시간을 가지게 되었습니다. 실험실 생활을 하면서 여러 면으로 미흡했던 제가 점점 연구자로서의 면모를 갖추게 되기까지는 주변을 여러 고마운 분들의 관심과 격려가 있었기 때문이라는 생각이 듭니다. 앞으로의 인생에서 많은 사람에게 도움을 주는 사람이 되어야겠다는 다짐을 확고히 하였으며, 그 동안 도움을 준 많은 사람께 진심으로 감사해야 함을 배웠습니다. 그리고 그 첫 실천으로 이번 박사학위 속 감사의 글을 통해 제게 은혜를 주신 분들께 감사의 마음을 전하고자 합니다.

가장 먼저 학부생 때부터 아낌없는 조언과 훌륭한 가르침을 주신 지도교수님이신 김현이 교수님께 진심으로 감사한 마음을 전하고 싶습니다. 저는 교수님에게서 제자에 대한 교수님의 깊은 애정을 느낄 수 있었고 연구자로서의 태도와 학습방법을 배울 수 있었습니다. 잦은 실수와 부족함에도 언제나 믿고 지켜봐 주신 덕분에 지금의 제가 있을 수 있던 것 같습니다. 제가 교수님을 만난 건 제 인생의 커다란 선물이었음을 고백합니다. 제가 예전에 했던 말처럼 저도 교수님처럼 꼭 ‘훌륭한’ 사람이 되도록 하겠습니다.

그리고 귀한 시간 허락해 주시고 논문 심사를 맡아주신

한홍남 교수님, 남기태 교수님께도 감사 드립니다. 학부 과정 및 대학원 과정 동안 교수님들의 수업과 관심, 지도 덕분에 많은 것을 배울 수 있었습니다. 앞으로도 심사위원들께서 해주신 말씀 잊지 않고 제 연구에 많은 도움이 되도록 하겠습니다.

다음으로 고영학 교수님께 진심으로 감사의 말씀을 드립니다. 바쁘신 와중에도 제 논문이 발전할 수 있게 함께 고민해주시고 지도해주셔서 감사합니다. 평소 교수님께서 보여주신 위트와 지도력 그리고 통찰력을 정말 배우고 싶습니다. 그리고 논문심사 때 해주신 칭찬과 격려의 말씀은 학문의 의미와 가치를 잊지 말라는 의미로 이해하고, 훌륭한 학자의 길을 걷는 것으로 보답하겠습니다.

그리고 이용호 박사님께 진심으로 감사의 말씀을 드립니다. 염치 없는 제 부탁을 들어 주시고, 제 논문의 부족함을 날카롭게 지적해주셔서 감사합니다. 덕분에 제 눈에 보이지 않는 많은 부족함을 수정할 수 있었습니다. 그리고 박사님께서 보여주신 온화한 마음과 학생을 존중하는 태도는 정말 큰 감동이었습니다.

Professor Juri Estrin, thank you for all the valuable comments and suggestions.

또한 대학원 입학 때부터 함께했던 SLIM 실험실 선배님들과 후배님들께 깊은 감사 드립니다. 우선 아무것도 모르고 처음 실험실에 인턴으로 들어 갔을 때 계시던 선배님들이 있습니다. 실험의 재미를 알게 해주신 김해원 교수님, 지금은 결혼을 하셔서 가정을 꾸리신 창번 형, 묵묵히 본인이 맡으신 일을 성실히 하시는 승호 형, 무서운 듯 하면서 재미있으신 치성 형,

남을 잘 배려하시는 재웅 형, 동근 형, 종재 형, 재료원리 수업 때
조교였던 주하 누나께 감사합니다.

졸업 후에도 연구에 도움을 주시고 애정으로 대해주신
병호 형에게도 감사합니다. 형의 조언을 통해 다양한 시각으로
연구를 하는 법을 배울 수 있었습니다. 항상 따끔한 충고와 직언을
해주신 성미 누나, 앞으로도 많은 가르침 부탁 드립니다. 지금의
생체 재료 실험실이 있기까지 초석을 놓아주셨던 은정 누나,
누나에겐 미안하고 감사할 따름입니다. 자상하고 온화하신 원영 형,
항상 하시는 일이 잘 되기를 바랍니다. 친 누나처럼 관심 가져
주시고 격려해주신 신희 누나, 이제 좋은 남자 만나 행복해질
시간입니다. 정신적 지주로서 많은 도움과 조언을 아끼시지 않은
지훈 형, 지금 계신 곳에서도 빛을 발할 것이라 믿습니다.

같이 실험실에 들어온 동기였던 홍지연, 차분하고
부끄러움이 많은 영호, 미친 성대모사로 사람들을 웃기는 봉규 형,
어디서나 적응 잘하고 다재 다능한 상복, 영어 잘하는 승희와 규란,
항상 호탕한 웃음으로 즐거운 분위기를 만들어 주신 창훈 형, 지금
있는 곳에서도 잘 해 나갈 수 있을 거라 믿고, 앞으로도 더 좋은
결과 만들어가길 바랍니다.

지금 실험실의 제일 큰 형님으로 지금도 후배들을 잘
챙겨주시는 세원 형, 졸업을 축하 드립니다. 성실한 연구 자세를
몸소 보여주신 철민 형, 부디 원하시는 꿈을 이루기를 바랍니다.
저의 가능성을 높이 사주신 종훈 형, 고난과 역경을 딛고 무슨
일이든 잘하실 것이라 믿습니다. 무슨 문제든 다 해결해주시던
해결사 원룡 형, 항상 가족의 평화와 안녕이 깃들길 바랍니다.

날카로운 눈을 가진 태식, 논문뿐만 아니라 발표 등 여러 가지 면에서 나의 부족함을 지적 받아 고칠 수 있었어. 넌 마성의 사나이가 될 자질이 충분해. 이번에 방장이 된 새미, 힘들겠지만 1년 동안 고생해주길 바래. Mathilde, si vous avez besoin de mon aide, n'hésitez pas à m'appeler. 조용히 자기할 일을 성실히 할 줄 아는 성원, 언젠가 티비에서도 볼 수 있기를 바래. 이번에 함께 졸업하는 내 실험 파트너 희선, 졸업을 해도 지금까지처럼 사이 좋게 지낼 수 있으면 좋겠어. 실험뿐만 아니라 실험 외적인 곳에서도 두각을 나타내는 민호, 하는 일이 다 왕대박 날 거야. 강한 카리스마의 소유자 설하, 좀 더 참을성을 가지고 매사에 임하면 너가 정말 원하는 것을 얻을 수 있을 거야. 명랑 쾌활한 재욱, 올해는 더 열심히 하는 모습 보일 거라 믿어. 미래가 더욱 기대되는 현찬, 지금까지처럼 하면 실험실을 이끌어 나가는 인재가 될 거야.

연구에 몰두할 수 있도록 안 보이는 곳에서 많은 지원을 해주신 임성은 씨와 박자혜 씨에게도 감사 합니다. 더불어 BIM 실험실에서 알게 모르게 도움을 주는 관하 형, 영욱 형, 안민경 씨, 인환이에게도 감사의 말을 전합니다.

논문을 쓰면서 많은 신뢰를 보여주고, 즐거움을 준 친구들에게도 감사함을 전합니다. 같은 길을 걸으면서 제일 가까운 곳에서 힘이 되는 덕황, 힘든 여건에서도 곳곳이 연구하는 의선, 항상 듬직한 모습을 보이는 훈휘, 벌써 아이 둘의 아빠가 된 동석, 타지에서 공부하고 있는 진혁, 대학교 생활을 즐겁게 해준 남기, 지금의 모습 변하지 않고 영원히 친하게 지내길 바랍니다.

어릴 때부터 친한 친구인 현일, 자주는 못 보지만 마음은 통하는 별남, 힘들고 괴로울 때 즐거움을 준 기수, 취직해서 바쁜 태영, 믿음과 우정이 영원히 변치 않기를 바랍니다.

그 밖에도 이름을 일일이 거론하지 못한 많은 소중한 인연 분께도 감사한 마음이 많습니다. 마지막으로 제 평생의 후원자이자 언제나 숭고한 사랑으로 저를 보살펴주시고 믿어주시는 부모님과 동생에게도 감사의 마음과 진심 어린 사랑의 마음을 전합니다.

"앞으로 20 년이 지나면 당신은 당신이 한 일보다는 하지 않은 일들 때문에 더 후회할 것이다. 그러니 닳을 올려 안전한 포구를 떠나라. 당신의 뜻에 무역풍을 가득 안고 출발하여 탐험하라, 꿈꾸라, 그리고 발견하라."

마크 트웨인의 이 글처럼 저는 앞으로도 탐험하며 꿈꾸고 발견하는 새로운 항해를 할 것입니다. 지켜봐 주십시오.

-2013년 1월 집에서